NAVAL POSTGRADUATE SCHOOL
MONTEREY, CALIFORNIA

THESIS

SCATTERING FROM ROUGH PLATES

by

John M. Waddell

September, 1995

Thesis Advisor: David C. Jenn

Approved for public release; distribution is unlimited.

DISCLAIMER NOTICE

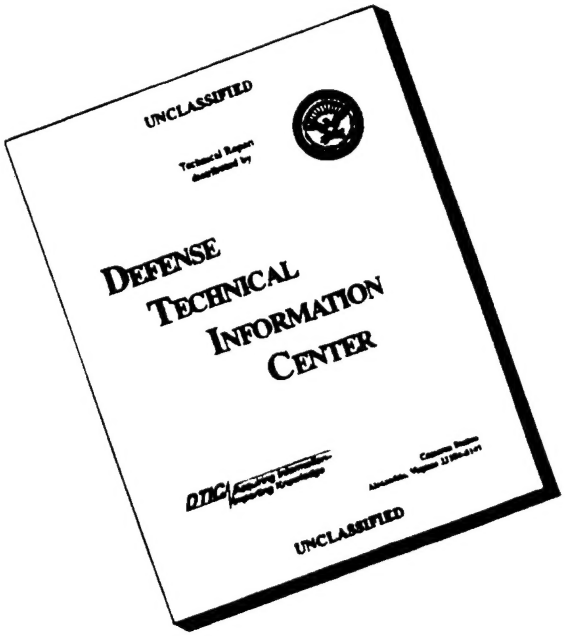

THIS DOCUMENT IS BEST QUALITY AVAILABLE. THE COPY FURNISHED TO DTIC CONTAINED A SIGNIFICANT NUMBER OF PAGES WHICH DO NOT REPRODUCE LEGIBLY.

REPORT DOCUMENTATION PAGE

Form Approved OMB No. 0704-0188

1. AGENCY USE ONLY *(Leave blank)*	2. REPORT DATE	3. REPORT TYPE AND DATES COVERED
	September 1995	Master's Thesis

4. TITLE AND SUBTITLE SCATTERING FROM ROUGH PLATES

5. FUNDING NUMBERS

6. AUTHOR(S) Waddell, John M.

7. PERFORMING ORGANIZATION NAME(S) AND ADDRESS(ES)
Naval Postgraduate School
Monterey CA 93943-5000

8. PERFORMING ORGANIZATION REPORT NUMBER

9. SPONSORING/MONITORING AGENCY NAME(S) AND ADDRESS(ES)

10. SPONSORING/MONITORING AGENCY REPORT NUMBER

11. SUPPLEMENTARY NOTES The views expressed in this thesis are those of the author and do not reflect the official policy or position of the Department of Defense or the U.S. Government.

12a. DISTRIBUTION/AVAILABILITY STATEMENT
Approved for public release; distribution is unlimited.

12b. DISTRIBUTION CODE

13. ABSTRACT *(maximum 200 words)*

The radar cross section (RCS) of rough rectangular plates was studied using Monte Carlo simulations with the method of moments (MM) and physical optics (PO), and by computing the mean power pattern. For both the MM and PO based simulations a plate in the xy plane is represented by a collection of small triangles. The roughness of the surface is obtained by randomly displacing the z coordinates of the triangle nodes. The main focus of the study was to look at the effects rough surfaces have on the off principal plane regions.

14. SUBJECT TERMS Radar Cross Section (RCS), Rough Surface Scattering, Method of Moments, Physical Optics

15. NUMBER OF PAGES 72

16. PRICE CODE

17. SECURITY CLASSIFICATION OF REPORT	18. SECURITY CLASSIFICATION OF THIS PAGE	19. SECURITY CLASSIFICATION OF ABSTRACT	20. LIMITATION OF ABSTRACT
Unclassified	Unclassified	Unclassified	UL

NSN 7540-01-280-5500

Standard Form 298 (Rev. 2-89)
Prescribed by ANSI Std. 239-18 298-102

Approved for public release; distribution is unlimited.

SCATTERING FROM ROUGH PLATES

John M. Waddell
GS-12/4, United States Air Force
B.E.E., Auburn University, 1988

Submitted in partial fulfillment
of the requirements for the degree of

MASTER OF SCIENCE IN ELECTRICAL ENGINEERING

from the

NAVAL POSTGRADUATE SCHOOL
September 1995

Author: 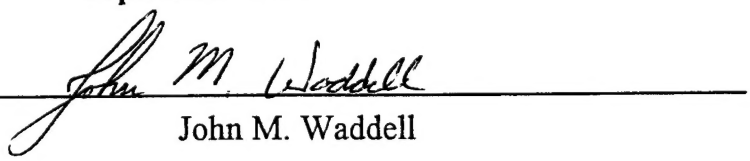
John M. Waddell

Approved by: 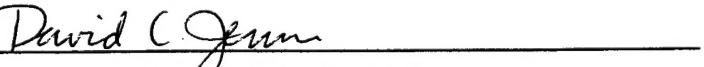
David C. Jenn, Thesis Advisor


Hung-Mou Lee, Second Reader

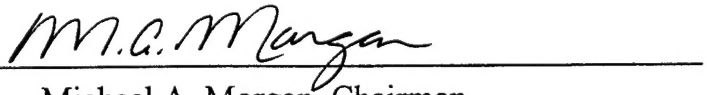
Michael A. Morgan, Chairman
Department of Electrical and Computer Engineering

ABSTRACT

The radar cross section (RCS) of rough rectangular plates was studied using Monte Carlo simulations with the method of moments (MM) and physical optics (PO), and by computing the mean power pattern. For both the MM and PO based simulations a plate in the xy plane is represented by a collection of small triangles. The roughness of the surface is obtained by randomly displacing the z coordinates of the triangle nodes. The main focus of the study was to look at the effects rough surfaces have on the off principal plane regions.

TABLE OF CONTENTS

I. INTRODUCTION

Since the invention of radar in World War II many applications have been found for its use in both the military and civilian sectors. Military radar applications include the detection and tracking of ships, aircraft and ground vehicles. Modern radar systems make it virtually impossible for ships and aircraft to approach targets without being detected at great distances. For this single reason, the military has put great emphasis on the lowering of the radar cross section (RCS) of military vehicles. The word stealth has been used by the media to describe specialized military vehicles specifically designed with a low RCS. In principle, a stealth vehicle can approach a radar without being detected, and thus has an increased probability of completing its mission objectives relative to a conventional vehicle.

Several factors contribute to the RCS of a vehicle. The shaping of its surfaces and the materials used in its construction have the most significant effect. The RCS of a rough surface can be significantly different from that of a smooth surface. A randomly rough surface reduces specular lobes and increases diffuse scattering. Diffuse scattering is not desirable because it is isotropic and, even though it has a very low level, it cannot be controlled by shaping. Surface roughness also affects the behavior of surface waves.

The sources of target surface imperfections are unavoidable. They arise from tolerances in the machining and assembly of parts, and in the fabrication of materials themselves. For example, the wing of an aircraft typically consists of a skin material laid over support structures. The

skin will have some deviation from the theoretical wing shape. Furthermore, if the skin is a composite material, its dielectric constant and loss tangent will not be precisely the same throughout the material. Thus the wing is a rough, inhomogeneous, anisotropic scatterer.

RCS prediction methods can be divided into two categories: 1) approximate methods such as physical optics (PO) and 2) rigorous methods such as integral equation techniques and the method of moments (MM). In this thesis both PO and MM are used to calculate the RCS of plates of various sizes, both perfectly flat and rough. For both of these methods the plate is represented using triangular patches. When MM is applied, the patches are the subdomains used in the current expansion. For the PO solution, closed-form expressions for scattering from a triangular plate are employed. The rough surface is obtained by selecting a random number at each node of the plate. The random deviations generated in this manner are scaled to produce a random surface of a specified variance. The usefulness of PO can be accessed by a comparison of the average RCS level with that obtained using MM. It is the average RCS level (or diffuse scattering) that is of interest in specifying tolerances on the manufacturing and assembly processes.

This thesis investigates the characteristics of electromagnetic scattering from surfaces with random roughness and its impact on RCS. The first objective is the comparison of the approximate and rigorous scattering analysis methods using a Monte Carlo simulation. The average RCS levels obtained from the Monte Carlo simulations are then compared to a closed-form expression for the mean power pattern derived by

Ruze (Ruze, 1952). The second objective is to investigate the effects of surface roughness on the RCS patterns; in particular, how it affects the specular, traveling wave, and diffuse RCS components.

Chapter II is a review of the Rayleigh Criterion and how rough surfaces affect specular and diffuse scattering. Also discussed is a method for the calculation of the mean power pattern using a statistical approach.

Chapter III reviews PO and MM. The analysis methods are presented and the required equations derived. Computer coding of the equations in MATLAB is also discussed.

Chapter IV is an evaluation of the data obtained from the computer models, primarily highlighting the differences in RCS patterns using the two analysis techniques. A summary consisting of the mean power patten difference as related to the roughness of the surface is presented. Chapter V summarizes the results and highlights the advantages and disadvantages of each approach as well as suggests possible future work.

II. THEORETICAL BACKGROUND

In this chapter the concepts and equations used to describe scattering from rough surfaces are introduced.

A. RAYLEIGH CRITERION

One of the first researchers to study the effects of scattering from rough surfaces was Rayleigh back in 1877. His approach was to look at a plane wave normally incident onto a sinusoidal surface. [Ref. 1] This approach led to the basis for determining the degree of roughness of a surface, now known as the Rayleigh criterion. Figure 1 shows a rough

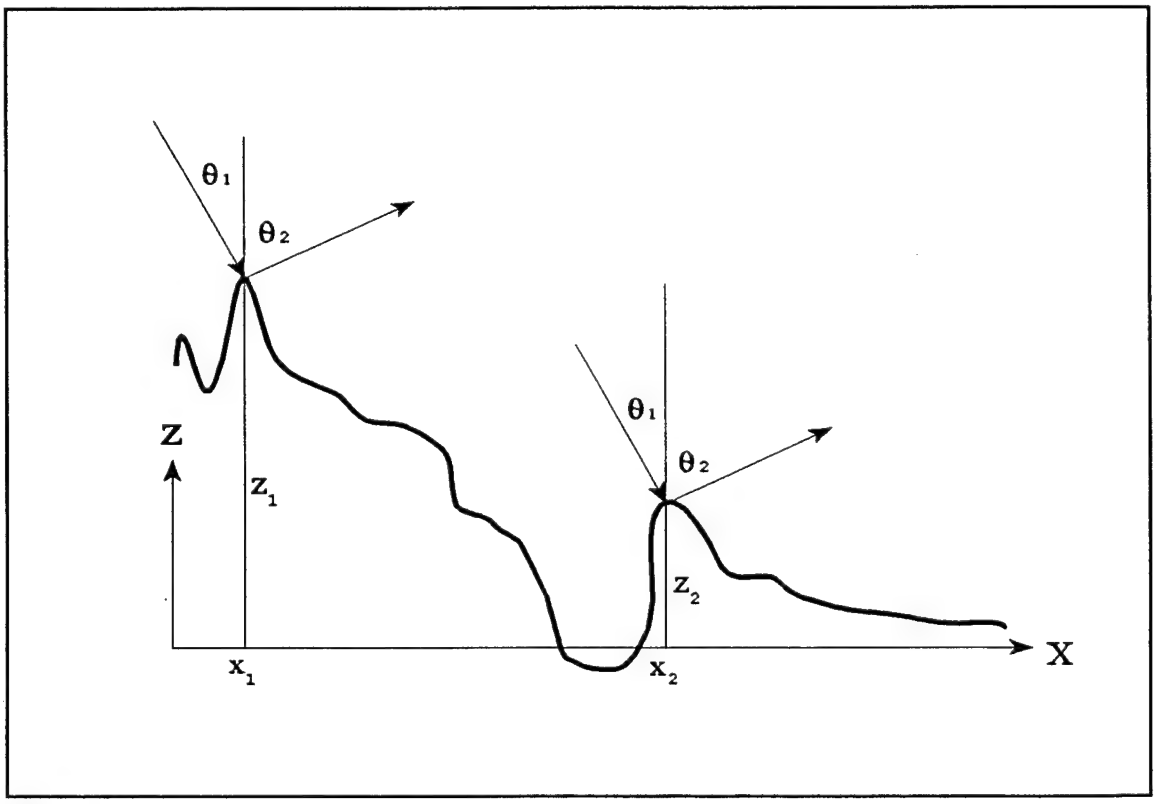

Figure 1. Rough surface diagram used to determine the phase difference between two parallel scattered rays. After Ref. [1].

surface with a plane wave incident from angle θ_1 in the x-z plane. The phase difference ($\Delta\phi$) between the two parallel rays scattered into the x-z plane from separate points can be calculated by

$$\Delta\phi = k[(z_1 - z_2)(\cos\theta_1 + \cos\theta_2) + (x_2 - x_1)(\sin\theta_1 - \sin\theta_2)] \qquad (2.1)$$

where the heights of the two separate scattering points are z_1 and z_2. In equation 2.1 the variable k represents the modulus of the incident and scattered wave vector ($k=2\pi/\lambda$). For specular scattering $\theta_1=\theta_2$ and the phase difference becomes

$$\Delta\phi = 2k(z_1 - z_2)\cos\theta_1 \, . \qquad (2.2)$$

The precise way in which the two scattered rays interact with each other depends on the value of $\Delta\phi$ relative to π. If $\Delta\phi \ll \pi$, then the two scattered waves are nearly in phase and thus interfere constructively; if $\Delta\phi \approx \pi$, then the two scattered waves interfere destructively. In the latter case there will be no contribution of scattered energy in the specular direction. [Ref. 1] The *Rayleigh criterion* is a commonly accepted definition of a rough surface: if $\Delta\phi < \pi$ then the surface is considered smooth, otherwise it is rough. For a continuous surface with many scattering points the root mean square (RMS) deviation $\bar{\delta}$ is used in place of z_1-z_2. Thus the Rayleigh criterion can be expressed as

$$R_a < \pi/4 \qquad (2.3)$$

where R_a is known as the Rayleigh parameter and is given by

$$R_a = k\delta\cos\theta_1 \ . \qquad (2.4)$$

The Rayleigh criterion can be used to illustrate the effects of a rough surface on an incident plane wave. If $z_1 = z_2$, then the phase difference becomes

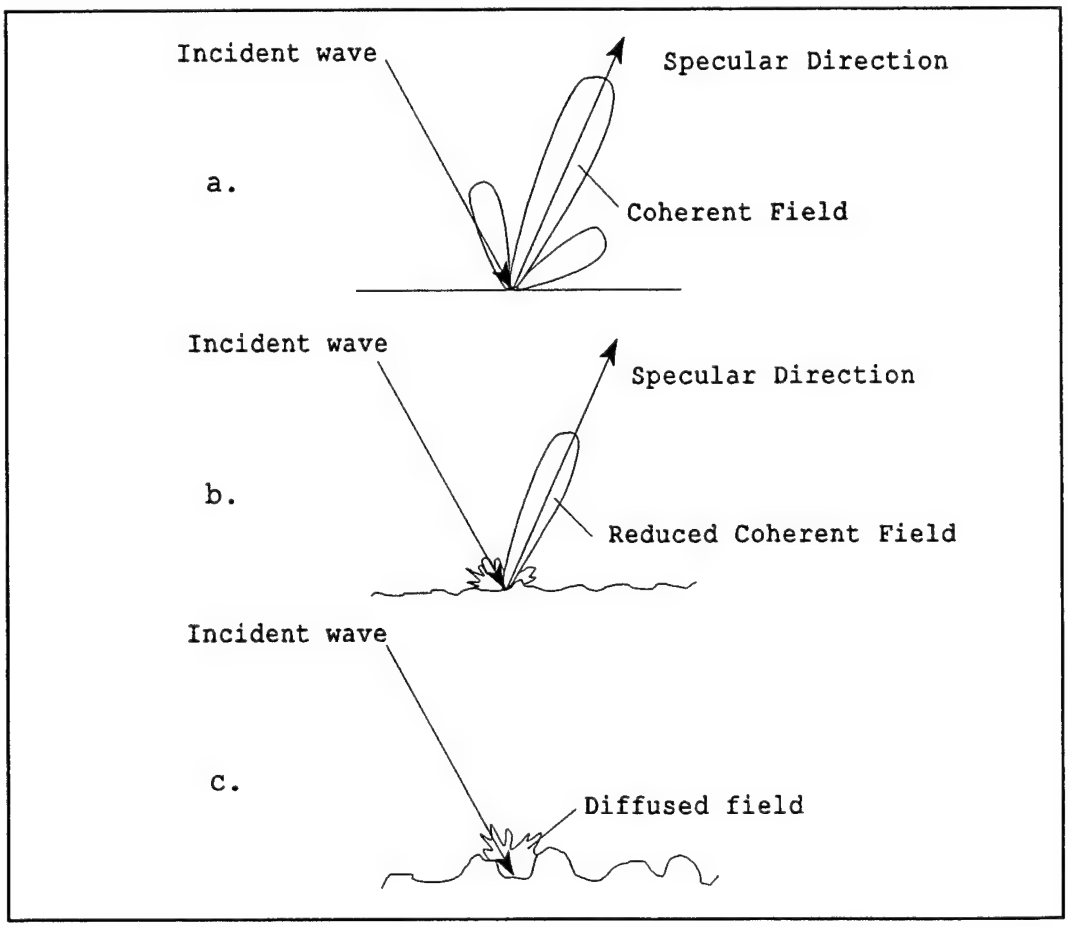

Figure 2. a) Scattering from smooth surface, b) scattering from a slightly rough surface, and c) scattering from a rough surface. These diagrams show how the degree of surface roughness reduces the scattering in the specular direction.

$$\Delta\phi = k(x_2 - x_1)(\sin\theta_1 - \sin\theta_2) \quad . \tag{2.5}$$

As shown in Figure 2, for a smooth plate of very large extent, the incident wave is almost completely scattered in the specular direction. However, if z_1 is not equal to z_2 the surface becomes rough and less energy is scattered in the specular direction. Equation 2.2 can be used to find the phase difference for the given surface and incident angle. When R_a is small compared to π, then the surface can be treated as though it were smooth. If the phase difference is no longer negligible, a significant amount of the incident energy is scattered diffusely. Finally, if the phase variation from point-to-point on the surface becomes large then diffuse scattering dominates. A perfectly diffuse surface is one that scatters uniformly in all directions for every incidence angle.

B. STATISTICAL APPROACH TO SOLID SURFACE SCATTERING

Ruze investigated the effects of random surface errors on the gain of reflector antennas using a statistical approach. [Ref. 2] It is possible to derive a closed-form expression for the mean power pattern from the radiation integrals for electromagnetic scattering. To derive the expression, some simplifying assumptions and approximations are made. One is that the surface bumps can be represented locally by a Gaussian shape as shown in Figure 3. The width of the Gaussion shape is characterized by a correlation interval, c. It is the average distance at which the deviation becomes uncorrelated. An easy way to explain large correlation interval is to imagine a slowly varying deviation as an

observer travels along the surface. On the other hand, a small correlation interval has a rapidly varying surface profile. Figure 3 gives examples of large and small correlation intervals.

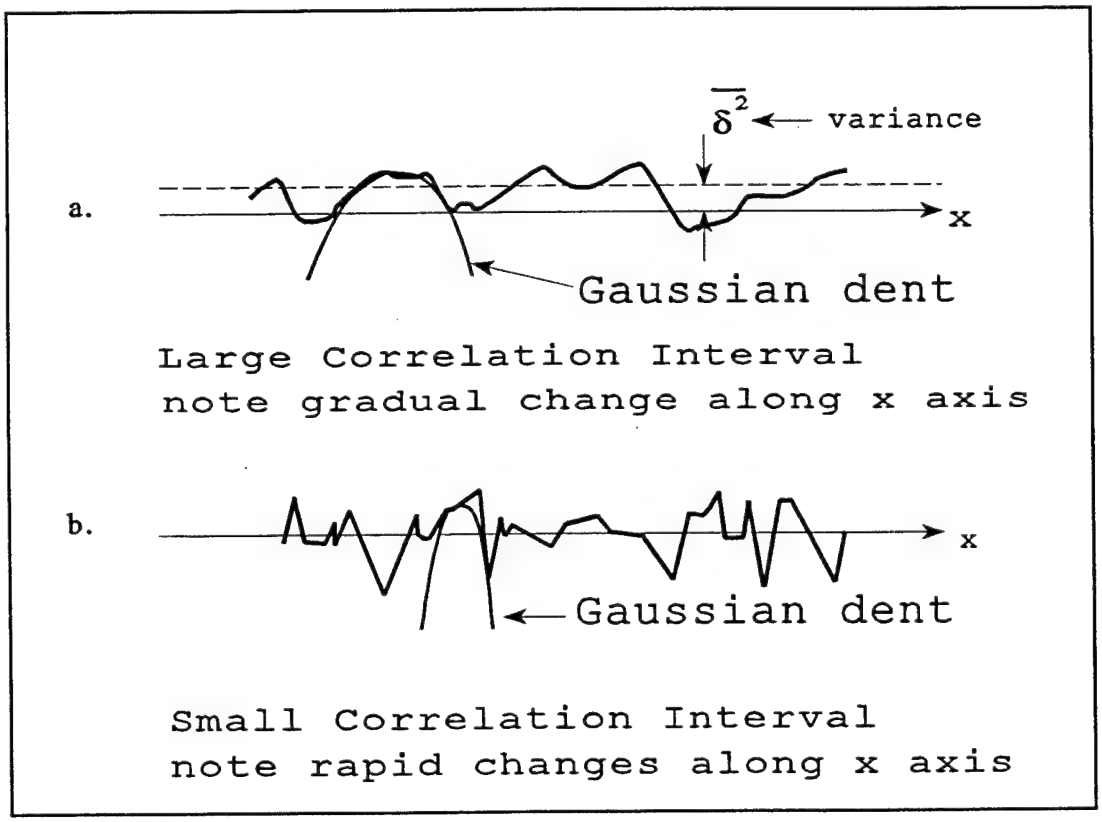

Figure 3. Rough surfaces with a) large correlation interval and b) small correlation interval.

A closed-form expression for the average RCS can be derived from the mean power pattern

$$< P >=< \bar{E}_r \cdot \bar{E}_r^* > \qquad (2.6)$$

where <·> denotes expectation. The complete derivation for

the mean power pattern can be found in Jenn [Ref. 3] and therefore only the highlights are presented here. Along with the gaussian approximation just described, a second assumption in the derivation of the closed form equation is that, as long as the roughness on the surface is sufficiently small, the z component of the surface current for a plate lying in the x-y plane can be neglected. Only the x and y components contribute to the scattered field. For an incident wave polarized transverse magnetic to the z-axis (TM_z)

$$J_x = -\frac{2e^{jkg}}{\eta_o} E_{0\theta}\cos\phi \qquad (2.7)$$

$$J_y = -\frac{2e^{jkg}}{\eta_o} E_{0\theta}\sin\phi$$

where $g=-\hat{k}\cdot\bar{r}'$, $\bar{k}=k(\hat{x}u+\hat{y}v+\hat{z}w)$, and $\bar{r}'=\hat{x}x'$ and $\hat{y}y'$. The quantities u, v, and w are the direction cosines of the observation point and are defined as: $u = \sin\theta\sin\phi$, $v = \sin\theta\sin\phi$, $w = \cos\theta$, and (θ,ϕ) gives the direction to the observation point. η_0 represents the impedance of free space.

The scattered field for a unit incident field ($E_{0\theta}=1$) is

$$E_{s\theta} = \frac{-jk\cos\theta e^{-jkr_0}}{2\pi r_0}\int\int_A e^{j2\bar{k}\cdot\bar{r}'} e^{j2k\delta(\bar{r}')} ds' \qquad (2.8)$$

where r_0 represents the distance from the local surface origin to the observation point. The surface devation as a function of position is $\delta(\bar{r}')$. Now using equation 2.8 in 2.6

$$< P >=< \bar{E}_s \cdot \bar{E}_s^* >= \left(\frac{k\cos\theta}{2\pi r_0} \right)^2 \iint_A \iint_A e^{j2\bar{k}\cdot(\bar{r}-\bar{r}')} < e^{jk[\delta(\bar{r})-\delta(\bar{r}')]} > ds'ds. \quad (2.9)$$

The error-free power pattern (i.e. pattern of a prefectly flat plate) is

$$P_0 = \left(\frac{k\cos\theta}{2\pi r_0} \right)^2 \iint_A \iint_A e^{j2\bar{k}\cdot(\bar{r}-\bar{r}')} ds'ds \ . \quad (2.10)$$

Taking the expected value of the exponential in equation 2.9, expanding the integrand in a Taylor Series, then breaking out the first term gives

$$<P> = \left(\frac{k\cos\theta}{2\pi r_0} \right)^2 e^{-4k^2\bar{\delta}^2} \left\{ P_o + \iint_A \sum_{n=0}^{\infty} \frac{(4k^2\bar{\delta}^2)^n}{n!} e^{-n\tau^2/c^2} e^{j2\bar{k}\cdot\bar{\tau}} ds'ds \right\} \quad (2.11)$$

where $\bar{\tau}=\bar{r}-\bar{r}'$ and $\bar{\delta}^2$ is the variance of the deviations. Switching to polar coordinates and extending the limits of the integration to infinity for reasons stated by Jenn [Ref. 3], equation 2.11 can be further reduced to

$$< P > = \left(\frac{k\cos\theta}{2\pi r_0} \right)^2 e^{-4k^2\bar{\delta}^2} \left\{ P_o + 4k^2\bar{\delta}^2 c^2 \pi A \exp\left(-\frac{c^2\pi^2\sin^2\theta}{\lambda^2} \right) \right\} \quad (2.12)$$

where A is the area of the plate.

The RCS, σ, can now be found in terms of the mean power pattern using the fact that the incident plane wave has unit amplitude. For large r_0

$$\sigma = 4\pi r_0^2 < P > . \quad (2.13)$$

Equation 2.10 can be normalized to the area squared

$$P_{norm} = \frac{P_o}{A^2} \tag{2.14}$$

and therefore equation 2.13 becomes

$$\sigma = \frac{4\pi A^2 \cos^2\theta}{\lambda^2} e^{-4k^2\bar{\delta}^2} \left\{ P_{norm} + \frac{4k^2\bar{\delta}^2\pi c^2}{A} \exp\left(-\frac{c^2\pi^2\sin^2\theta}{\lambda^2} \right) \right\}. \tag{2.15}$$

The second term in equation 2.15 represents the average or diffuse RCS level. Because the variance is present in the second term, it shows the importance of maintaining tight surface tolerances.

A similar calculation can be performed for a two dimensional array of discrete isotropic scatterers that are randomly dislocated from the z=0 plane. The mean power pattern consists of two terms similar to equation 2.15. The first is the error-free pattern, which depends on the array factor of the scatterers. The second term is

$$\sigma = \frac{4\pi A^2}{\lambda^2} \left(\frac{\cos^2\theta(4k\cos^2\theta\bar{\delta}^2)}{MN} \right) \tag{2.16}$$

where MN is the total number of scatterers making up the array. Equation 2.16 represents the average RCS level. It is

interesting to note that if the discrete array has a rectangular grid spaced dx by dy, its area is $MNdxdy$. Equating the second term of equation 2.15 to equation 2.16 gives

$$dxdy = \pi c^2 \,. \tag{2.17}$$

Thus an equivalent correlation interval for the discrete array can be computed.

III. METHOD AND FORMULATIONS

The equations required for the PO and MM Monte Carlo simulations are developed in this chapter. Also introduced is a brief description of the computer code used in the simulation.

A. PHYSICAL OPTICS (PO)

Probably the most commonly used prediction method for the study of wave scattering from rough surfaces is the physical optics approximation. [Ref. 1] Physical optics provides an estimate of the surface current on the illuminated part of the target. The shadowed area is assumed to have a surface current of zero. One limiting factor that should be mentioned is that the use of physical optics will not show the effects of traveling waves that normally appear along the edges of surfaces. Surfaces that are terminated with edges, as in the case of a rectangular plate, have traveling waves reflected back towards the source. Thus for monostatic RCS calculations, PO can give erroneous results at angles near surface grazing.

The derivation of the scattered fields for physical optics begins with the geometrical optics approximation of the surface current on the illuminated portion of the body. The surface current is

$$\bar{J}_s \approx \begin{cases} 2\hat{n} \times \bar{H}_i, & \textit{for illuminated part of the body,} \\ 0, & \textit{for shadowed part of the body.} \end{cases} \qquad (3.1)$$

In equation 3.1, $\bar{H}_i$ is the incident magnetic field intensity at the surface and $\hat{n}$ is the surface normal vector. Now

consider a flat plate of dimensions a and b as shown in Figure 4. An incident wave has arbitrary polarization defined by the constants $E_{0\theta}$ and $E_{0\phi}$, and is incident from a direction given by the angles (θ,ϕ):

$$\bar{E}_i=(E_{0\theta}\hat{\theta}+E_{0\phi}\hat{\phi})e^{-j\bar{k}_i\cdot\bar{r}}\ . \tag{3.2}$$

The magnetic field intensity can be written as

$$\bar{H}_i=-(E_{0\theta}\hat{\phi}-E_{0\phi}\hat{\theta})\frac{e^{-j\bar{k}_i\cdot\bar{r}}}{\eta_0} \tag{3.3}$$

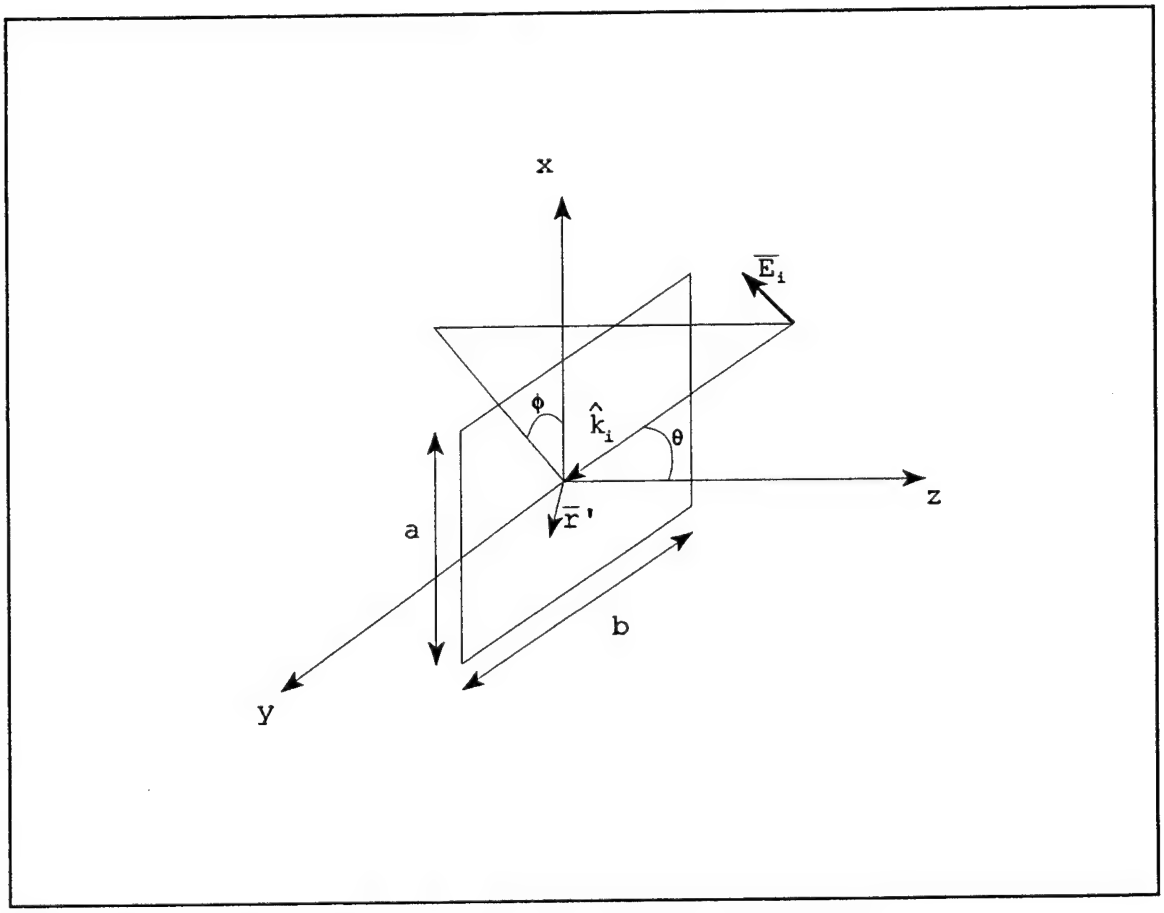

Figure 4. Plane wave scattering by a flat plate.

provided that the wave is propagating towards the origin. Now substituting the magnetic field intensity into equation 3.1 it is possible to approximate the surface current of the rectangular plate

$$\bar{J}_s \approx -2\hat{n} \times (E_{0\theta}\hat{\phi} - E_{0\phi}\hat{\theta})\frac{e^{j\bar{k}_i \cdot \bar{r}}}{\eta_0} . \tag{3.4}$$

For a flat plate in the x y plane, equation 3.4 becomes

$$\bar{J}_s \approx 2\hat{z} \times \left[(\hat{\theta}E_{0\phi} - \hat{\phi}E_{0\theta})\frac{e^{jkg}}{\eta_0}\right] \tag{3.5}$$

where $g = x'u + y'v + z'w$.

Finally, the monostatic scattered field can be determined from the surface current

$$\bar{E}_s = \frac{jk\eta_0}{4\pi r_0}\int\int_A \bar{J}_s \, e^{jkh} ds' . \tag{3.6}$$

Combining equations 3.5 and 3.6 gives

$$\bar{E}_s = \frac{jk}{2\pi r_0} e^{-jkr_0}(\hat{z} \times [\hat{\theta}E_{0\phi} - \hat{\phi}E_{0\theta}])\int\int_A e^{jk(g+h)} ds' \tag{3.7}$$

where A is the total area of the plate and $g = h$ for the monostatic case.

A rough plate can be represented by a collection of triangular patches. The edges of adjacent triangles touch, but

the normals point in different directions as evident in Figure 5. Thus the total integral in 3.7 is a sum of integrals, each over a single triangle

$$I=\iint_A e^{j2kg}ds'=\sum_{i=1}^{N_t}\iint_{A_i} e^{2kg}ds\equiv\sum_{i=1}^{N_t} I_i \qquad (3.8)$$

where N_t represents the total number of triangles on the plate and I_i is the ith integration result. The closed-form expressions for I_i are derived by Moreira and Prata. [Ref. 4] In general,

$$I_i=2A_i e^{jD_0}\left(e^{jD_p}\left[\frac{C_R+C_0}{D_p(D_q-D_p)}+F_1-F_2\right]-e^{jD_q}\left[\frac{C_q+C_0}{D_q(D_q-D_p)}-F_2\right]-\frac{C_0}{D_pD_q}-F_1\right) \qquad (3.9)$$

where A_i is the area of the triangular cell. Figure 6 shows the integration cell geometry used in equation 3.9. For plane wave incidence

$$C_p=A_{i,1}-A_{i,3}=0, \qquad C_q=A_{i,2}-A_{i,3}=0, \qquad C_0=A_{i,3}, \quad F_1=0,$$
$$D_p=k(B_{i,1}-B_{i,3}), \qquad D_q=k(B_{i,2}-B_{i,3}), \qquad D_0=kB_{i,3}, \quad F_2=0.$$

$A_{i,m}$ and $B_{i,m}$ represent the amplitude and phase of the integrand at node m of triangle i, respectively, as shown in Figure 6. Equation 3.9 can be reduced to

$$I_i=2A_i e^{jD_0}\left(e^{jD_p}\left[\frac{C_0}{D_p(D_q-D_p)}\right]-e^{jD_q}\left[\frac{C_0}{D_q(D_q-D_p)}\right]-\frac{C_0}{D_pD_q}\right) . \qquad (3.10)$$

Equation 3.10 has some removable singularities that cause problems numerically when $|D_p|$, $|D_q|$ and $|D_q-D_p|$ are small. These singularities are handled as special cases and expressions are derived by expanding the integrand in a Taylor

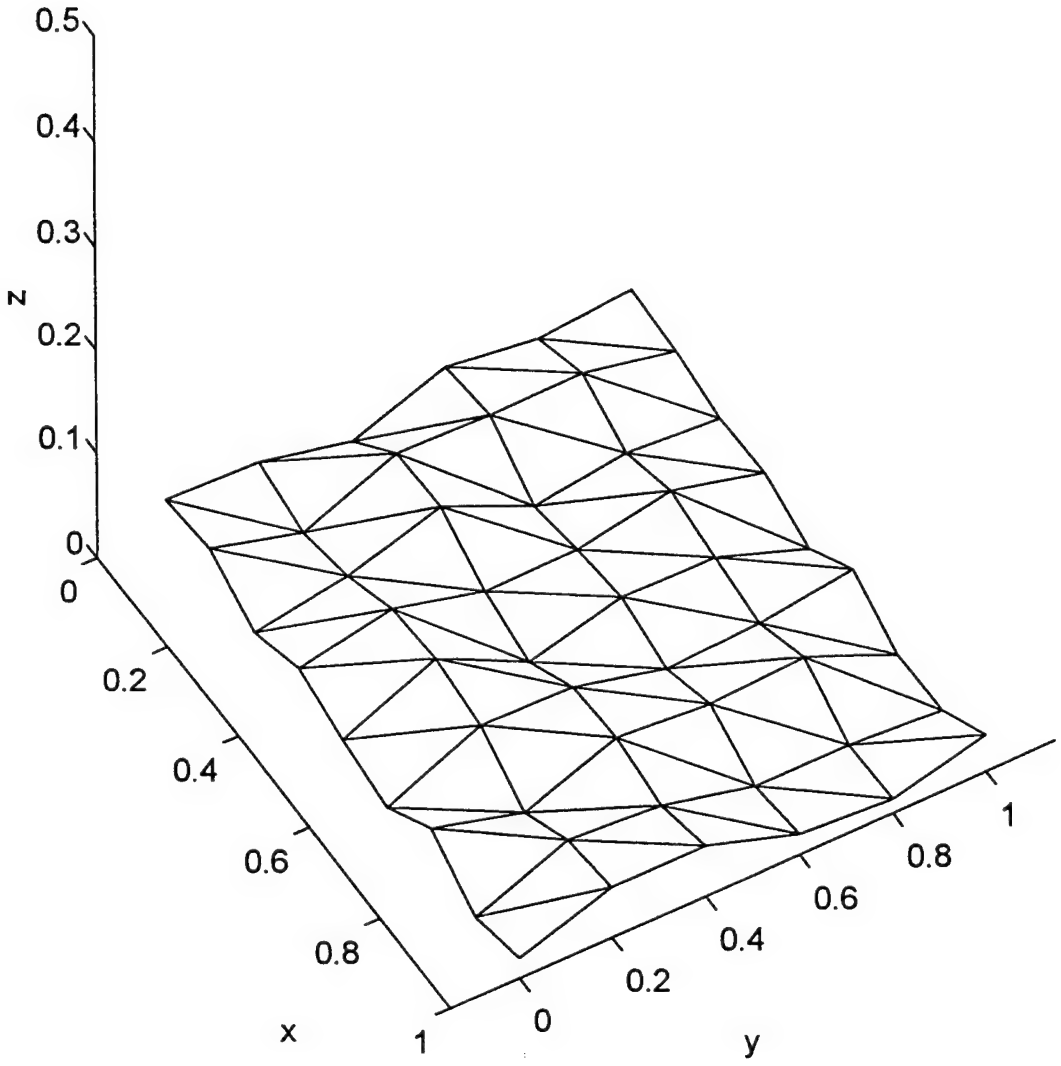

Figure 5. Triangular patch model of a rough scattering surface.

series and analytically integrating the resultant series term by term. The following special cases result [Ref. 4]:

1. If $|D_p|<L_t$ and $|D_q|\geq L_t$ (no restrictions on $|D_q-D_p|$)

$$I_i=2A_i\frac{e^{jD_0}}{jD_q}\sum_{n=0}^{\infty}\frac{(jD_p)^n}{n!}\left(\frac{1}{n+1}(-C_0)+e^{jD_q}\left[C_0G(n,-D_q)+C_p-C_q)G(n+1,-D_q)\right]\right) \quad (3.11)$$

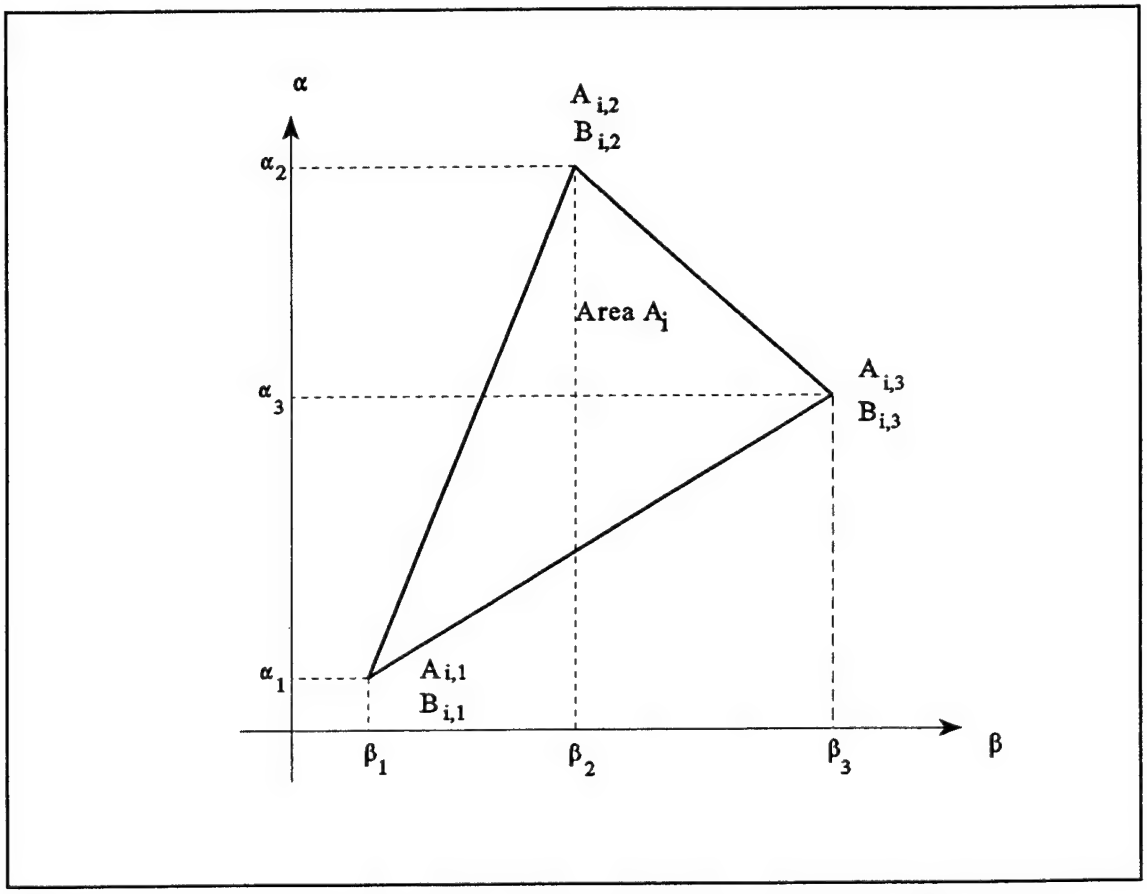

Figure 6. Integration cell geometry in local coordinates.

2. If $|D_p|<L_t$ and $|D_q|<L_t$ (no restrictions on $|D_q-D_p|$)

$$I_i=2A_i e^{jD_0}\sum_{n=0}^{\infty}\sum_{m=0}^{\infty}\frac{C_0(jD_p)^n(jD_q)^m}{(n+m+2)!} . \tag{3.12}$$

3. If $|D_p|\geq L_t$ and $|D_q|<L_t$ (no restrictions on $|D_q-D_p|$)

$$I_i=2A_i e^{jD_0}e^{jD_p}\sum_{n=0}^{\infty}\frac{(jD_q)^n}{n!}\left(\frac{C_0}{n+1}\right)G(n+1,-D_p) . \tag{3.13}$$

4. If $|D_p|\geq L_t$ and $|D_q|\geq L_t$ and $|D_q-D_p|<L_t$

$$I_i=2A_i\frac{e^{jD_0}}{jD_q}\sum_{n=0}^{\infty}\frac{|j(D_p-D_q)|^n}{n!}\left[-C_0G(n,\ D_q)+C_0\frac{e^{jD_q}}{n+1}\right] . \tag{3.14}$$

The function G is defined as

$$G(n,\alpha)=\int_0^1 s^n e^{j\alpha s}ds \tag{3.15}$$

and can be evaluated recursively using the relationship

$$G(n,\alpha)=\frac{e^{j\alpha}-nG(n-1,\alpha)}{j\alpha} ,\quad for\ n\geq 1 , \tag{3.16}$$

and

$$G(0,\alpha)=\frac{(e^{j\alpha}-1)}{j\alpha} . \tag{3.17}$$

As noted by Moreira, equation 3.16 is numerically efficient

and, accurate results are obtained in most cases by setting L_t=.05 and using $n, m \leq 2$. However for the rough plate it was found that L_t=.001 was required to avoid spikes in the RCS pattern. Finally, the RCS of the plate can be calculated from

$$\sigma = 4\pi r_0^2 \frac{|\bar{E}_s|^2}{|\bar{E}_i|^2} \tag{3.18}$$

and by using equation 3.7 and 3.8 to determine the scattered field.

B. COMPUTER SIMULATION USING PHYSICAL OPTICS

The rough surfaces used for the computer calculations in this thesis were created using MBUILD. It is written in FORTRAN, and can generate basic surfaces and then approximate them with triangular facets. The output is a data file consisting of the *x*, *y*, and *z* node locations of each facet. The *z* node is then randomly displaced to generate a rough surface of specified standard deviation. For the physical optics approximation, this data file is then broken up into various MATLAB files consisting of individual *x-y-z* points, edges, vertices, and faces.

The physical optics approximation calculation was done in MATLAB. The code is designed to present the user a three dimensional plot of the RCS pattern in direction cosine space. Equations 3.10 through 3.14 are functions of the local coordinate angles and, therefore, to use these equations, a transformation must be performed for each triangle as shown in the Figure 7. The transformation involves rotating about the

z axis to the plane defined by $\hat{z}$ and $\hat{n}$, and then rotating through the angle between $\hat{z}$ and $\hat{n}$ in that plane.

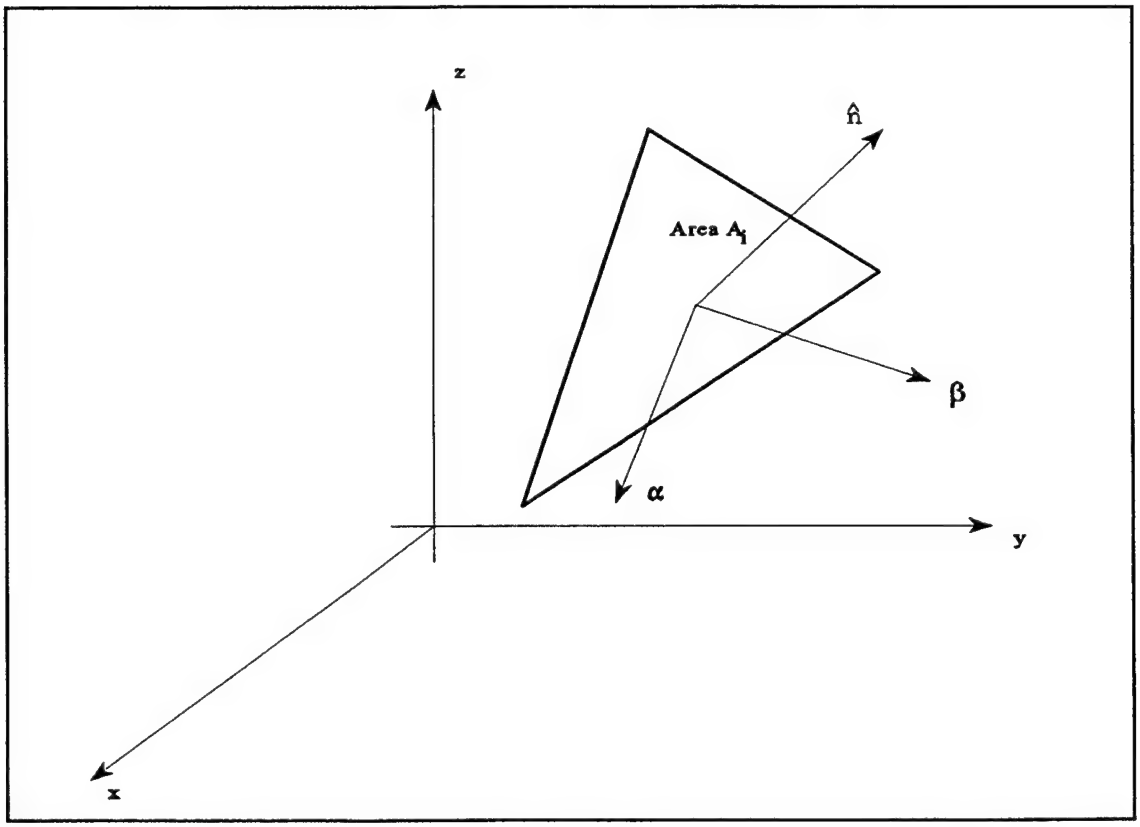

Figure 7. Translation of coordinates for a plate triangle.

C. METHOD OF MOMENTS (MM)

MM is a numerical technique that is very powerful because it can be applied to arbitrary bodies. Basically MM reduces an integral equation to a matrix problem. The matrix dimensions are dependent on the size of the scattering body in terms of the incident wavelength. For this reason the application of MM is limited to small and moderate target

sizes. The integral equation to be solved is the E-field integral equation (EFIE)

$$\bar{E}_i(\bar{r})|_{\tan} = \iint_S j\omega\mu \bar{J}_s(\bar{r}')G(\bar{r}, \bar{r}') - \frac{j}{\omega\epsilon}[\nabla'\cdot\bar{J}_s(\bar{r}')]\nabla' G(\bar{r}, \bar{r}')]_{\tan} ds' \,. \qquad (3.19)$$

In this chapter, S denotes the surface of integration.

The MM solution begins by representing the surface current by a series with unknown expansion coefficients, I_n:

$$\bar{J}_s = \sum_{n=1}^{N} I_n \bar{J}_n(\bar{r}) \,. \qquad (3.20)$$

$\bar{J}_n$ are the basis function, and both I_n and $\bar{J}_n$ can be complex. An important consideration in the MM solution is the selection of the basis functions. One should chooses a basis function that has the behavior expected of the current and minimizes computational effort. These functions are typically pulses, triangles, sinusoids and δ functions.

The next step is to solve for the series coefficients. Define a set of weighting functions W_m, m=1,2,...N. It is convenient to choose the complex conjugate of the basis function being used; this choice is referred to as *Galerkin's method.* [Ref. 3] The EFIE is multiplied by each weighting function and integrated over the domain resulting in N equations of form

$$\iint_{S_m} \bar{W}_m(\bar{r})\cdot\bar{E}_i(\bar{r})|_{\tan} = \iint_{S_m} \bar{W}_m(\bar{r})\cdot\left\{\sum_{n=1}^{N} I_n \times \right. \qquad (3.21)$$

$$\left. \iint_{S_n}\left[j\omega\mu\bar{J}_n(\bar{r}')G(\bar{r}, \bar{r}') - \frac{j}{\omega\epsilon}\nabla'\cdot\bar{J}_n(\bar{r}')\nabla' G(\bar{r}, \bar{r}')\right]_{\tan} ds'\right\} ds$$

for m=1,2...N. An impedance element can be defined between testing function m and the current basis function n

$$Z_{mn} \equiv \int\int_{S_m} ds \int\int_{S_n} ds' \left[\omega \mu \bar{W}_m(\bar{r}) \cdot \bar{J}_n(\bar{r}') \right. \tag{3.22}$$

$$\left. - \frac{j}{\omega \epsilon} \left(\nabla' \cdot \bar{J}_n(\bar{r}')\right) \left(\nabla \cdot \bar{W}_m(\bar{r})\right) \right] G(\bar{r}, \bar{r}') \ .$$

The right side of equation 3.21 is a voltage

$$V_m \equiv \int\int_S \bar{W}_m(\bar{r}) \cdot \bar{E}_i(\bar{r}) ds \ . \tag{3.23}$$

Using these definitions, equation 3.21 can be written as

$$V_m = \sum_{n=1}^{N} I_n Z_{mn} \qquad for\ m = 1,2,..,N \ . \tag{3.24}$$

Equation 3.24 can now be presented in matrix form as

$$V = ZI \tag{3.25}$$

I is a vector containing the unknown expansion coefficients. Z is the impedance matrix and V is the excitation vector. By inverting the matrix Z, I can be solved for:

$$I = Z^{-1} V. \tag{3.26}$$

Having evaluated the I_n, equation 3.20 is now defined and can be used in the radiation integral (equation 3.6).

A *measurement matrix*, R can be defined with elements

$$R_n = \iint_{S_n} \bar{J}_n(\bar{r}) \cdot \bar{E}_r(\bar{r}) ds \tag{3.27}$$

where $\bar{E}_r$ is a unit radiated plane wave. [Ref. 3] Using a θ polarized wave

$$\bar{E}_r = \hat{\theta} e^{-j\bar{k}_r \cdot \bar{r}} = \hat{\theta} e^{-jkr_0} e^{jkg}. \tag{3.28}$$

Combining equations 3.27 and 3.28

$$R_n^{\theta} = \iint_{S_n} [\hat{\theta} \cdot \bar{J}_n(\bar{r})] e^{jk(xu+yv+zw)} ds \tag{3.29}$$

where the superscript θ is added to denote the polarization of $\bar{E}_r$. Note that u, v, and w are the direction cosines for the observation direction. The same can be done for a ϕ polarized plane wave. The electric field components are

$$E_{\theta} = \frac{-jk\eta}{4\pi r_0} e^{-jkr_0} \sum_{n=1}^{N} R_n^{\theta} I_n \tag{3.30}$$

and for ϕ

$$E_{\phi} = \frac{-jk\eta}{4\pi r_0} e^{-jkr_0} \sum_{n=1}^{N} R_n^{\phi} I_n . \tag{3.31}$$

Referring to Figure 5, the rectangular plate is broken up into a collection of triangular faces. The surface current is represented by equation 3.20 where $\bar{r}$ is a position vector to a source point. Figure 8 shows the patch geometry for two

triangles with one common edge. The number of basis functions used is dependent on the number of edges shared with other triangles. If a patch has two shared edges, then it is spanned by two basis functions; a patch with three shared edges would be spanned by three basis functions. In Figure 8,

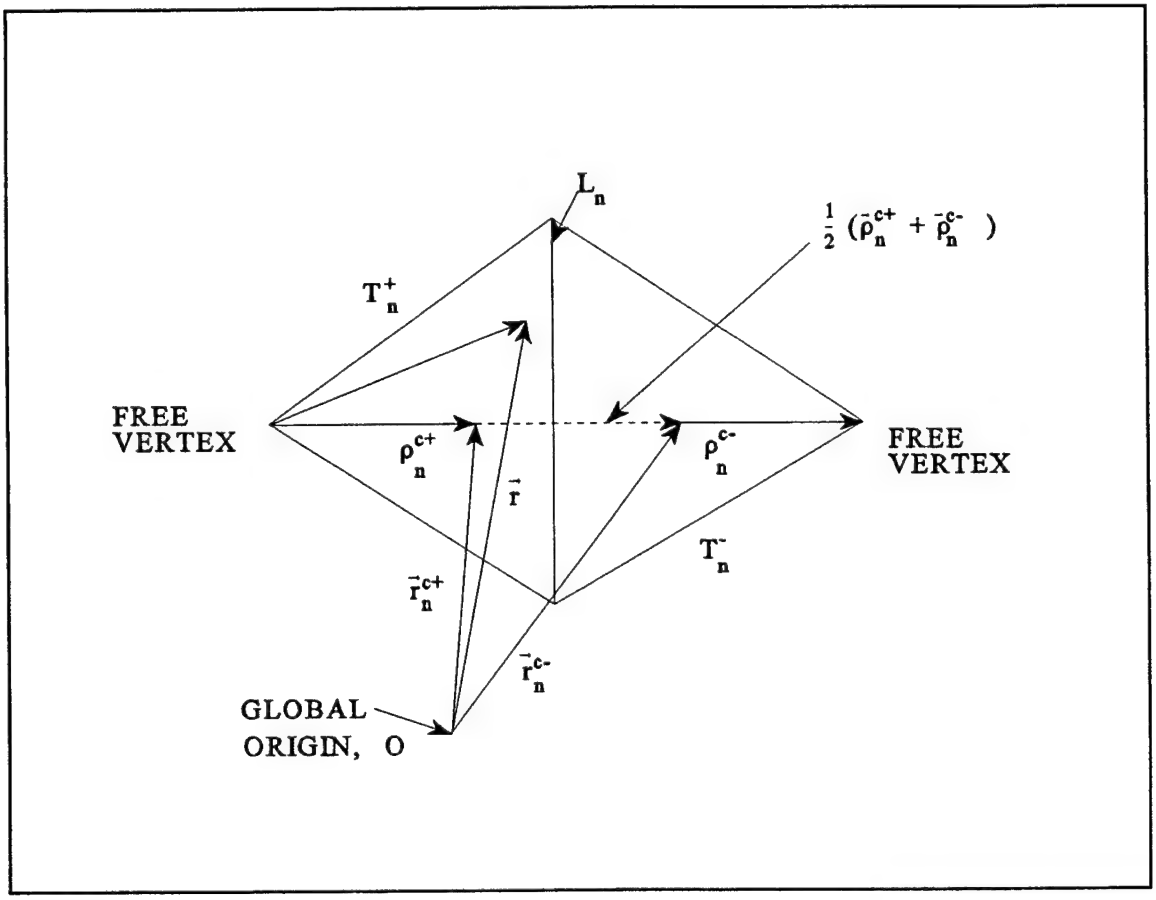

Figure 8. Triangular patch geometry.

edge n is shared by two triangular patches, T_n^+ and T_n^- with areas A_n^+ and A_n^-. The shared edge has a length of L_n. The vector basis function is written as

$$\bar{J}_n = \begin{cases} \dfrac{L_n \bar{\rho}_n^+}{2A_n^+}, & \bar{r} \text{ in } T_n^+ \\ \dfrac{L_n \bar{\rho}_n^-}{2A_n^-}, & \bar{r} \text{ in } T_n^- \end{cases} . \tag{3.32}$$

Some characteristics of these functions are: 1) for triangular edges that represent body edges, there is no normal component of the surface current, 2) the current normal to an internal edge n is constant and continuous across the edge, and 3) the divergence of $\bar{J}_n$ exists and has the expression

$$\nabla \cdot \bar{J}_n = \begin{cases} \dfrac{L_n}{A_n^+}, & \bar{r} \text{ in } T_n^+ \\ -\dfrac{L_n}{A_n^-}, & \bar{r} \text{ in } T_n^- \end{cases} . \tag{3.33}$$

The MM impedence elements can now be written as

$$Z_{mn} = L_m \left[\frac{j\omega}{2} (\bar{A}_{mn}^+ \cdot \bar{\rho}_m^{c+} + \bar{A}_{mn}^- \cdot \rho_m^{c-}) + \Phi_{mn}^- - \Phi_{mn}^+ \right] \tag{3.34}$$

where

$$\bar{A}_{mn}^{\pm} = \frac{\mu}{4\pi} \int\int_{S_n} \bar{J}_n(\bar{r}') \frac{e^{-jkR_m^{\pm}}}{R_m^{\pm}} ds' \tag{3.35}$$

$$\Phi_{mn}^{\pm} = \frac{-1}{4\pi j\omega\epsilon} \int\int_{S_n} \nabla' \cdot \bar{J}_n(\bar{r}') \frac{e^{-jkR_m^{\pm}}}{R_m^{\pm}} ds' \tag{3.36}$$

where $R_m^{\pm}=|\bar{r}_m^{c\pm}-\bar{r}'|$. The excitation vector elements are

$$V_m=L_m(\bar{E}_m^{+}\cdot\bar{\rho}_m^{c+}+\bar{E}_m^{-}\cdot\bar{\rho}_m^{c-}) \tag{3.37}$$

where the incident field is evaluated at the centroid

$$\bar{E}_m^{\pm}=\bar{E}_s(\bar{r}_m^{\pm}). \tag{3.38}$$

Using the expression for the impedance elements in 3.34, the integrals must be evaluated numerically. This should be accomplished by transforming to a set of localized coordinates on each patch and defining a set of normalized coordinates as in the case of PO. Singularity correction of the self term $(m=n)$ of the impedance matrix is generally required.

D. COMPUTER SIMULATION USING MM

The MM code used to simulate the varying rough surface was a code written by Sandia National Laboratories called PATCH. [Ref. 5] The output from the code provides the user with the currents coefficients and radar cross sections. PATCH uses the geometry file generated by MBUILD, which was previously discussed. Minor modifications were made to PATCH to calculate the RCS pattern of the rough surfaces in direction cosine space for comparison with the PO results.

IV. SUMMARY OF RESULTS

A. ROUGH SURFACE PLATE MODELS

The surfaces considered in all the simulations are 3λ by 3λ square plates. This was the largest plate possible given computer limitations. A large plate is desirable so that the principle plane sidelobes fall off rapidly, thus allowing the diffuse RCS of the off principal planes to dominate. Another limitation was the computer run time.

The FORTRAN code MBUILD was used to construct a plate comprised of 1800 triangles as shown in Figure 9. The plate node coordinates were then altered to produce the rough surfaces shown in Figure 10 and Figure 11. Figure 10 has a surface deviation uniformly distributed from 0 to 0.1λ with a mean of 0.05λ and, Figure 11 has deviation varying from 0 to 0.2λ with a mean of 0.1λ. The reason for the 0.1λ and 0.2λ deviations was to create a significant effect on the RCS pattern in the off principal plane regions. The manipulation of the *z* coordinates was done using a FORTRAN program ZCHN which generates a uniform random number from 0 to 1 and then is scaled based on the desired maximum amplitude deviation. Thus three plates are used in the simulation models in order to study their effects on RCS patterns.

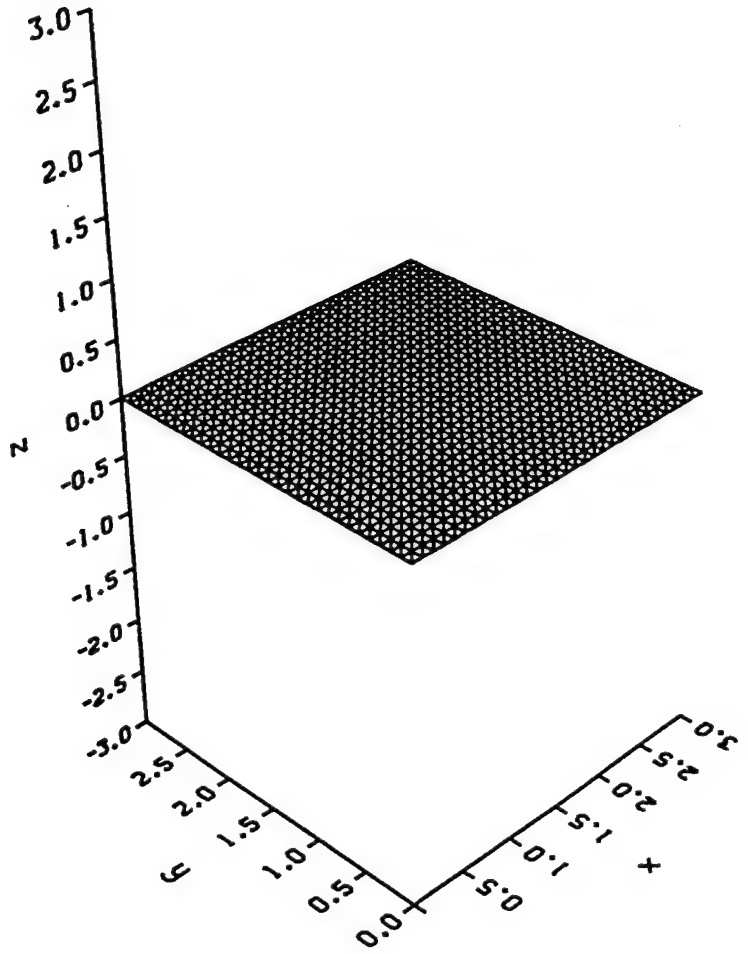

Figure 9. Flat plate 3.0λ by 3.0λ.

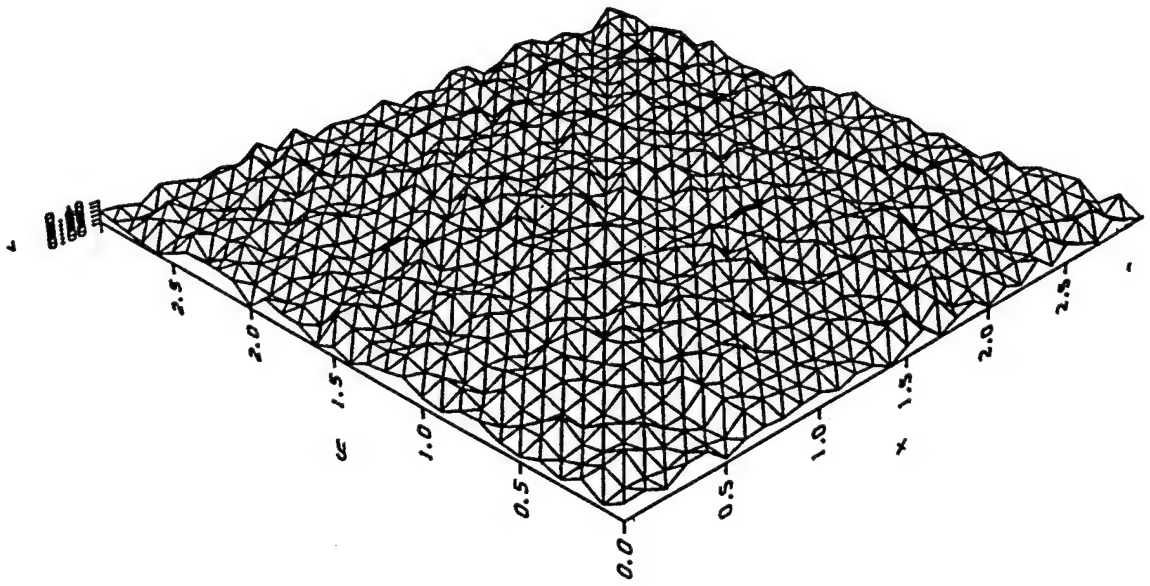

Figure 10. Rough plate with 0.1λ maximum surface deviation.

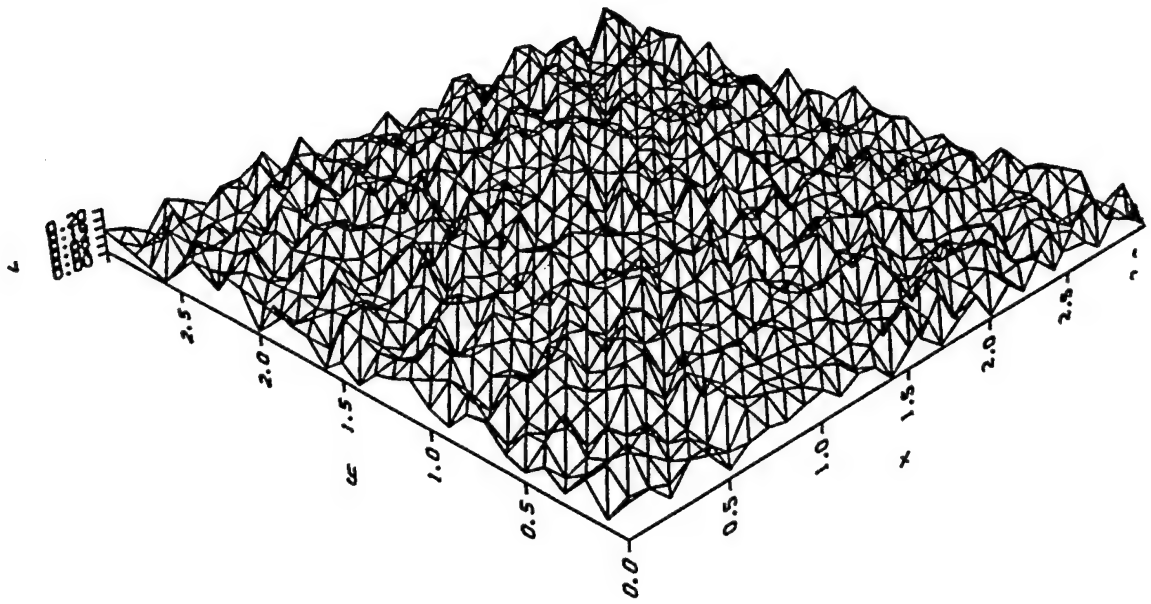

Figure 11. Rough plate with 0.2λ maximum surface deviation.

B. METHOD OF MOMENTS RESULTS

Method of moments is a rigorous solution of the scattering equations and therefore includes the effects of traveling waves. The software used to calculate the RCS patterns was PATCH. Figure 12 shows the RCS pattern for a flat 3λ by 3λ plate. The traveling waves cause the high RCS levels present around the edges of the pattern. The main lobe and principal plane side lobes are quite noticeable, but the off principal plane lobes are not as well defined because of the traveling wave. When the surface roughness is increased to 0.1λ, as in Figure 13, the principal plane lobes become less distinguishable because diffuse scattering raises the average level. Increasing the roughness to 0.2λ , as shown in Figure 14, results in a relatively uniform RCS level everywhere except the main lobe. Even the traveling wave effects have been reduced by the rough surface. In Figure 15, a cut is shown for u=-0.27. It illustrates the effect of the surface roughing: the principal plane lobes are decreased and the off principal plane lobes are increased.

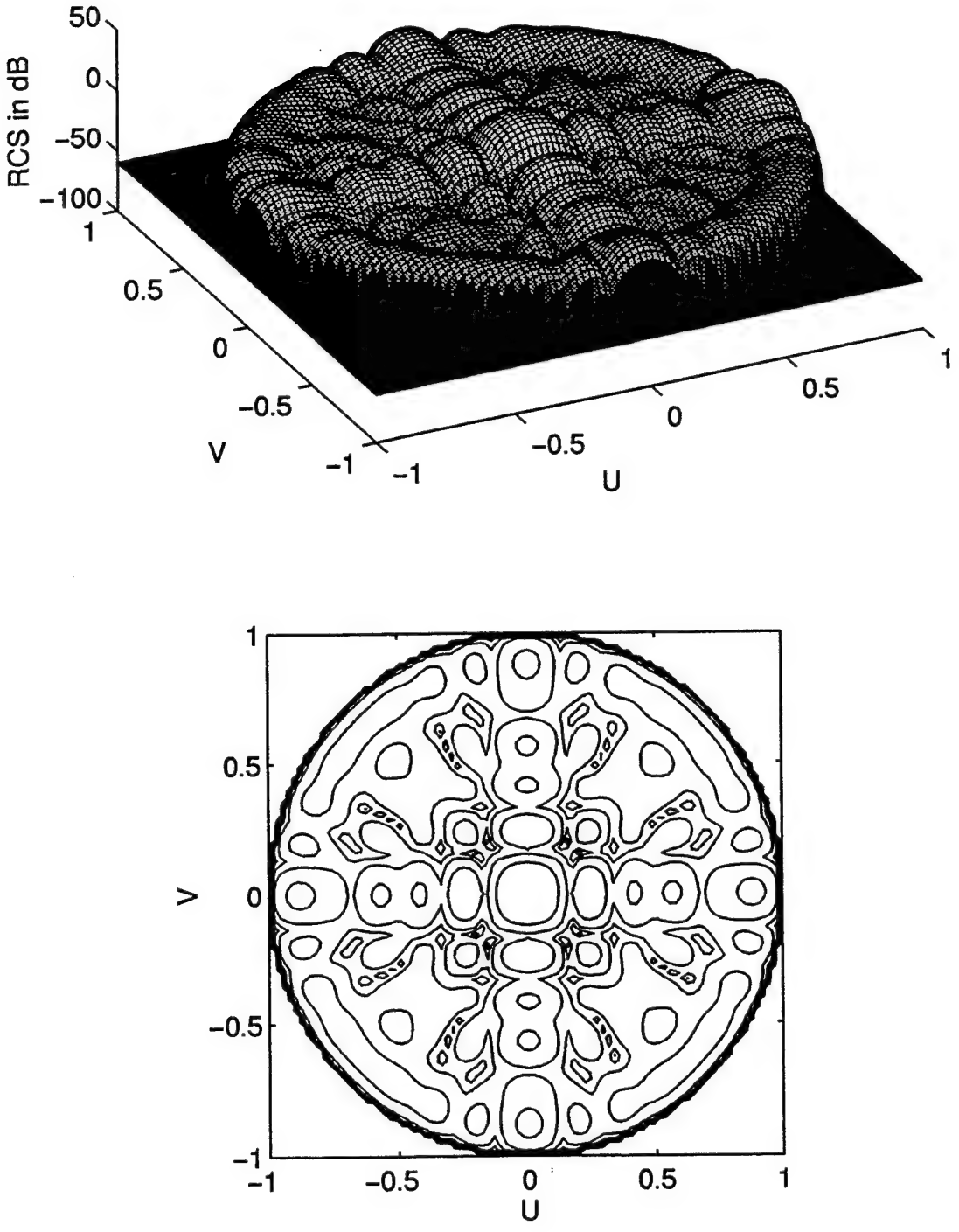

Figure 12. RCS of a flat plate computed using method of moments (3λ by 3λ).

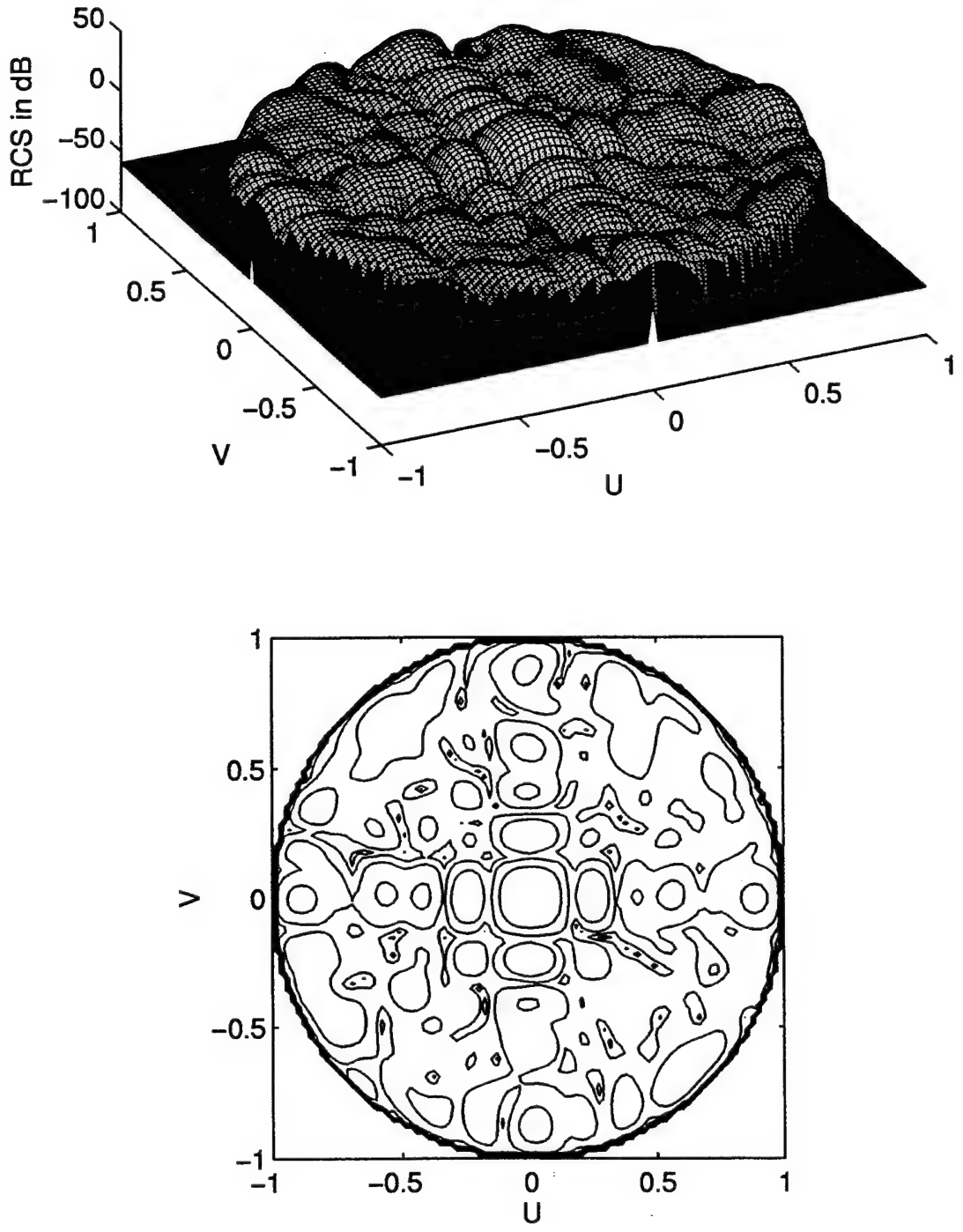

Figure 13. RCS of a rough plate computed using method of moments (3λ by 3λ, variance = 0.817e-3, and δ_{max}=.1λ).

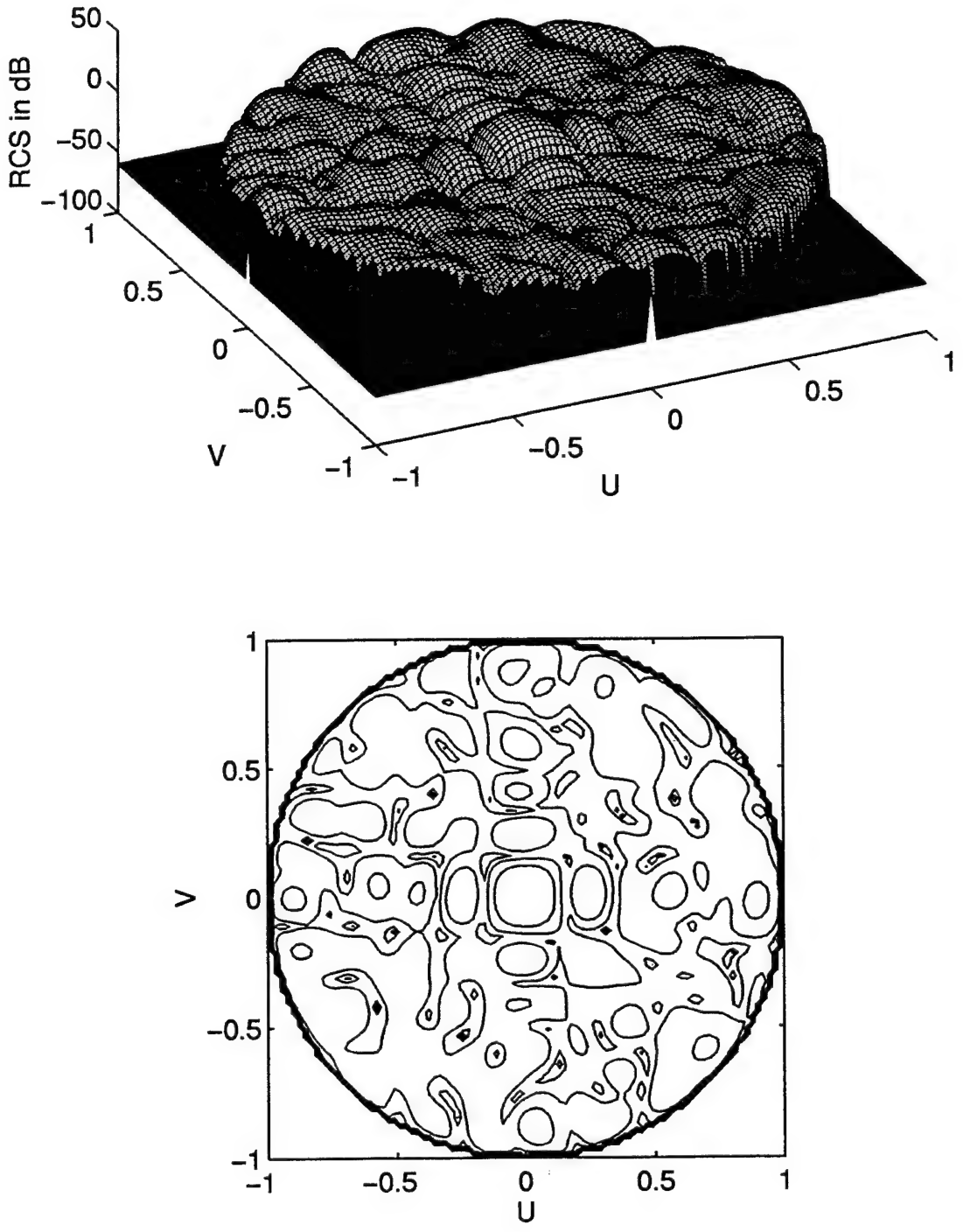

Figure 14. RCS of a rough plate computed using method of moments (3λ by 3λ, variance = 3.271e-3, and δ_{max}=.2λ).

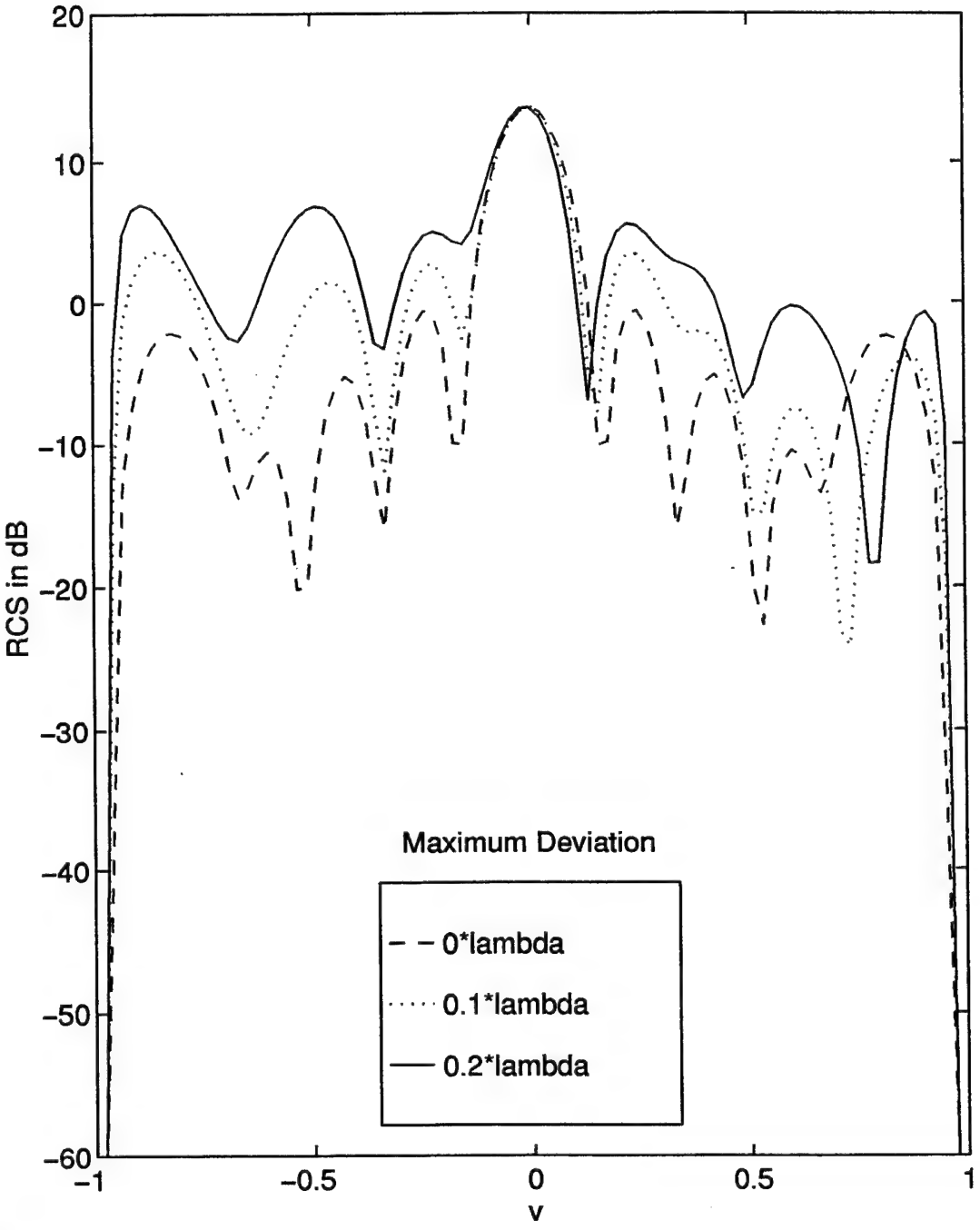

Figure 15. Plate RCS patterns computed using method of moments (3λ by 3λ and u = -0.27).

C. PHYSICAL OPTICS RESULTS

Using the MATLAB code POCOS, the RCS of 3λ by 3λ plates where plotted in direction cosine space for comparison with the MM data. Figure 16 shows a RCS pattern for a flat plate using the PO approximation. Because PO does not include traveling waves, the RCS levels around the edge of the pattern are noticeably lower than those of MM. The periodicity of the lobes is apparent when the RCS is plotted in direction cosine space. Figures 17 and 18 show the RCS patterns for the rough plates ($\bar{\delta}_{max}$ = 0.1λ and 0.2λ). The effects of random errors are more noticeable in this case than they are for MM because of the absence of traveling waves. As the surface roughness increases, the off principal plane lobes increase, and, if the roughness increases without bound, the scattering from the plate would become completely diffuse. A comparison of the rough surface patterns are shown in Figure 19. A cut of the RCS pattern has been taken at u=-0.27. Figure 19 shows the effect of the surface roughing. The off principal plane levels in some areas increase by as much as 35dB, while principal plane levels decrease only slightly.

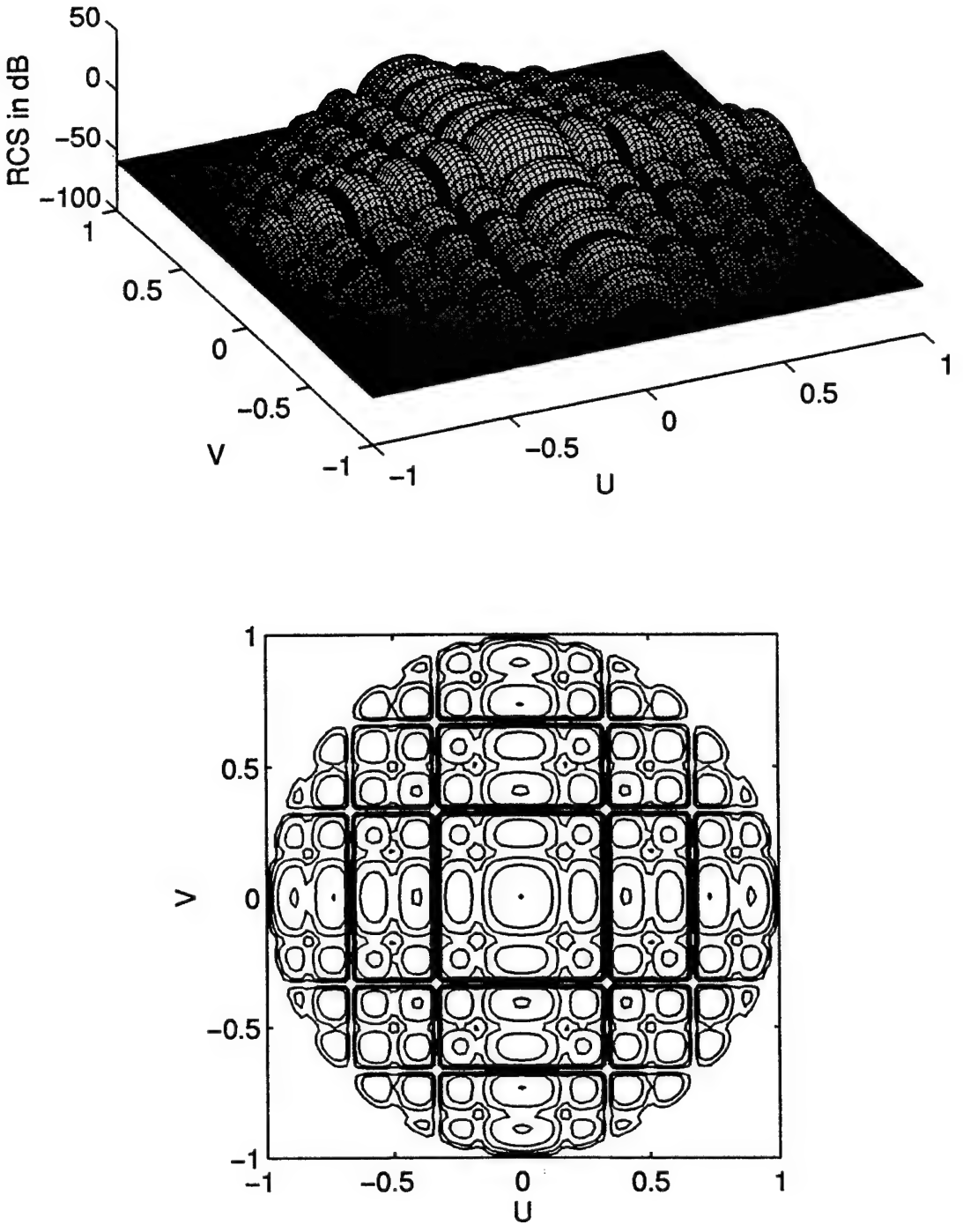

Figure 16. RCS of a flat plate computed using physical optics (3λ by 3λ).

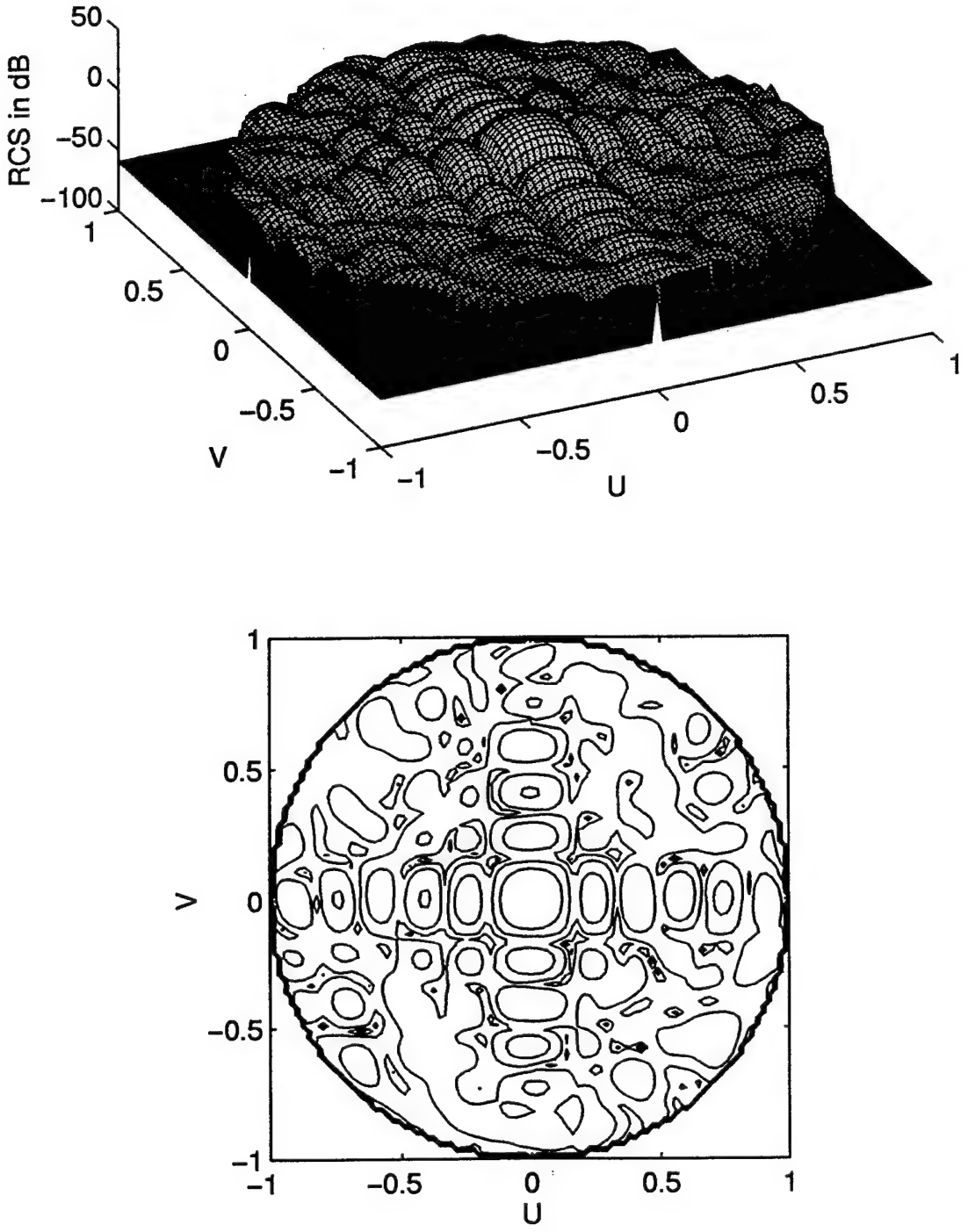

Figure 17. RCS of a rough plate computed using physical optics (3λ by 3λ, variance = 0.817e-3, and δ_{max}=.1λ).

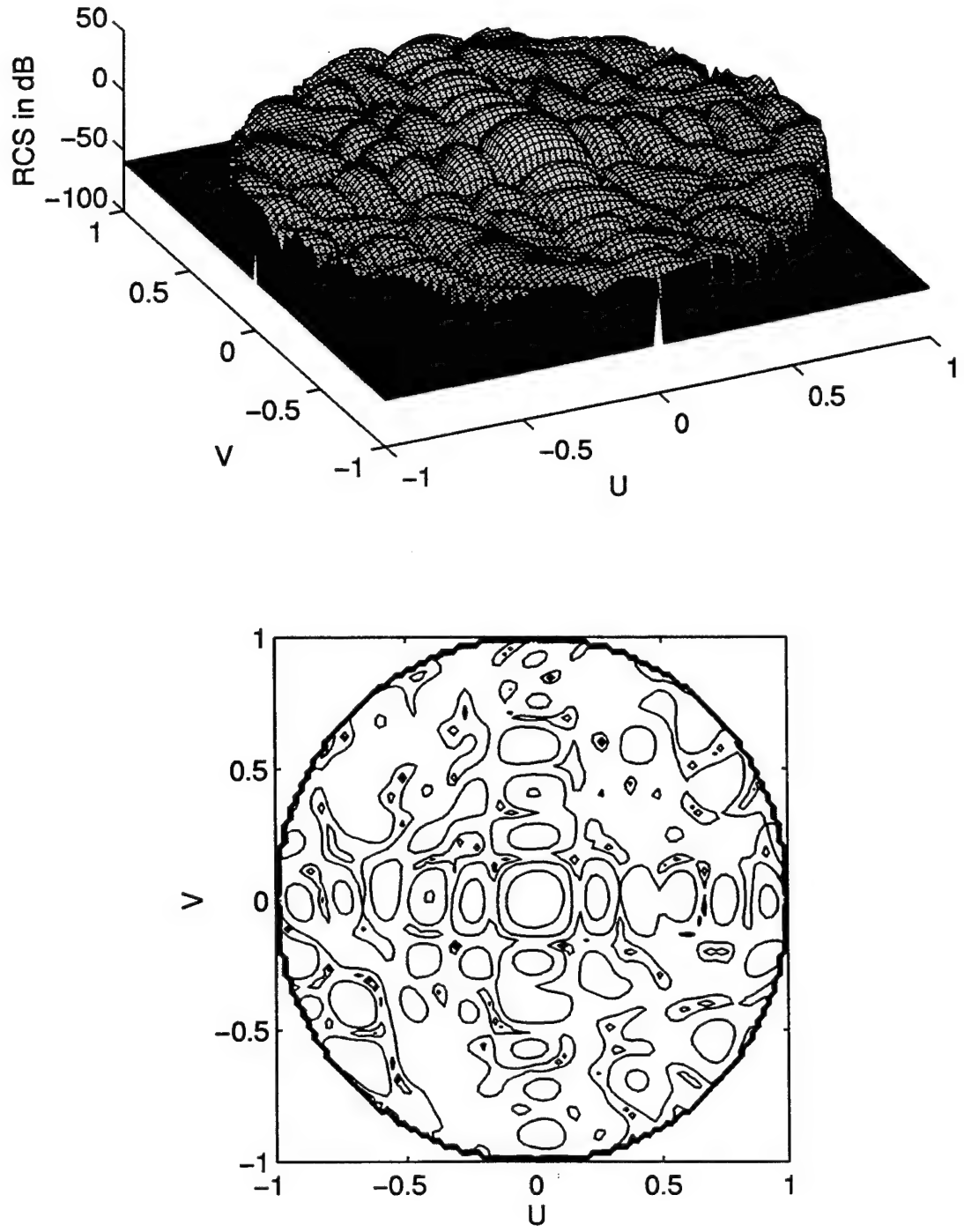

Figure 18. RCS of a rough plate computed using physical optics (3λ by 3λ, variance = 3.271e-3, and δ_{max}=.2λ).

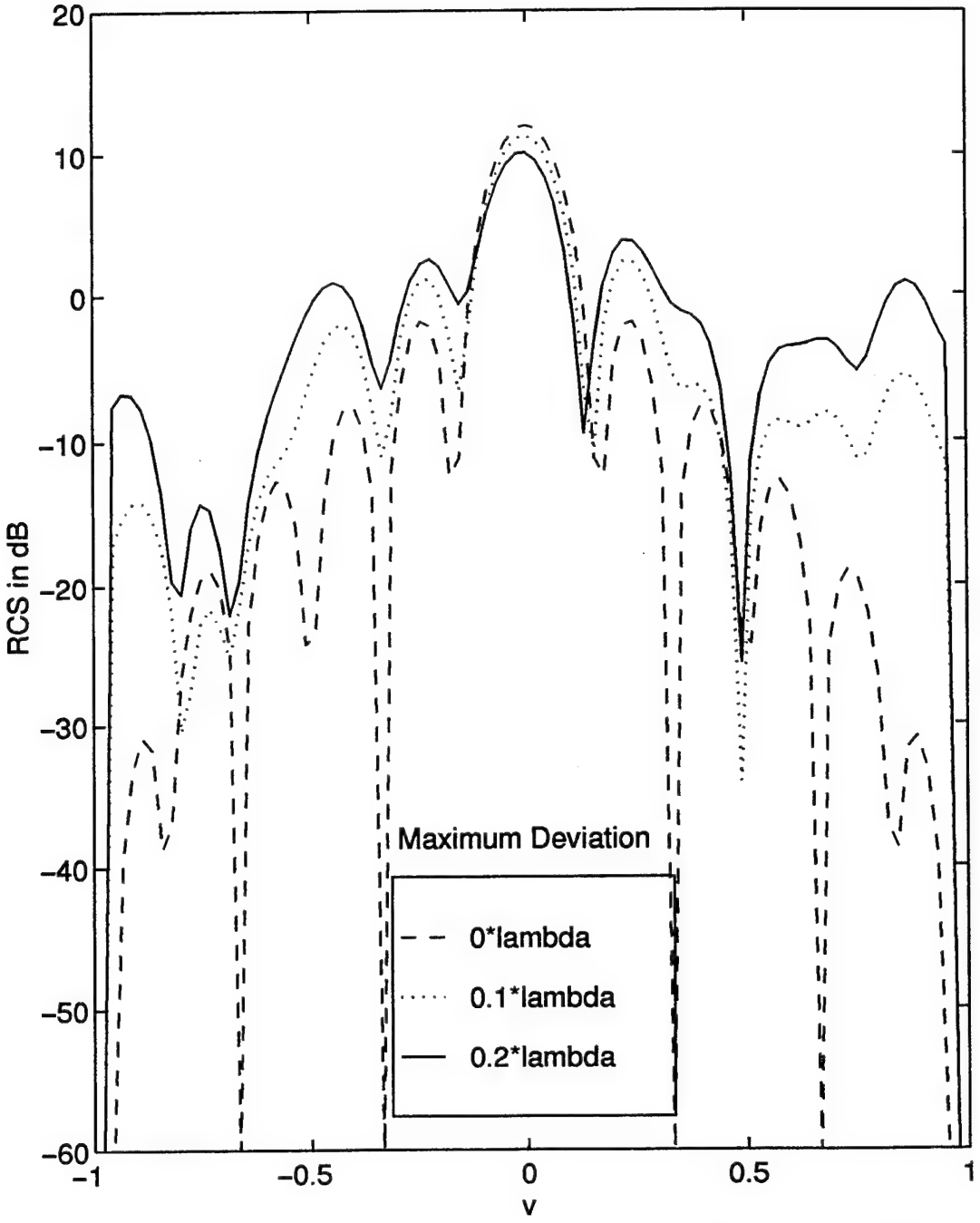

Figure 19. Plate RCS patterns computed using physical optics (3λ by 3λ and u = -0.27).

D. COMPARISON OF THE METHODS

The closed-form approximation, equation 2.15, can be used to calculate the average RCS level based on the area, variance, and correlation interval of the plate surface. The second term in equation 2.15 is plotted in Figures 20 and 21. The curves for several correlation intervals are shown. The MM and PO RCS curves are averaged over the four quadrants. Furthermore values of $|u|<0.2$ and $|v|<0.2$ where discarded when averaging, because the RCS in these regions is dominated by the specular RCS (ie., first term in equation 2.15). Surface roughness is not as noticeable in the MM plot because the surface wave scattering dominates at wide angles, even off the principal planes. The PO patterns illustrate that the diffuse scattering does dominate over the specular scattering at wide angles ($\theta \geq 40°$).

The plate nodes are located every 0.1λ in the x and y directions, and the roughness is achieved by randomly choosing the z coordinate at each node. Therefore, a first order estimate of the correlation interval might be $c=0.1\lambda$. This value gives curves too high relative to PO, which is the best indicator of the diffuse level (because it has no traveling waves). From the curves shown in the figures, it appears that the correlation interval is actually less, perhaps 0.07λ. This is close to the result obtained equating the second terms of equations 2.15 and 2.17. From equation 2.17

$$c^2 = \frac{(0.01\lambda)^2}{\pi} \qquad (4.1)$$

or

$$c \approx 0.06\lambda \ .$$

Note that the error terms represent the average levels due to surface roughness. The RCS has a Rayleigh probability density function and it is expected that ninety-eight percent of the sidelobes will be less than this average value plus 6dB.

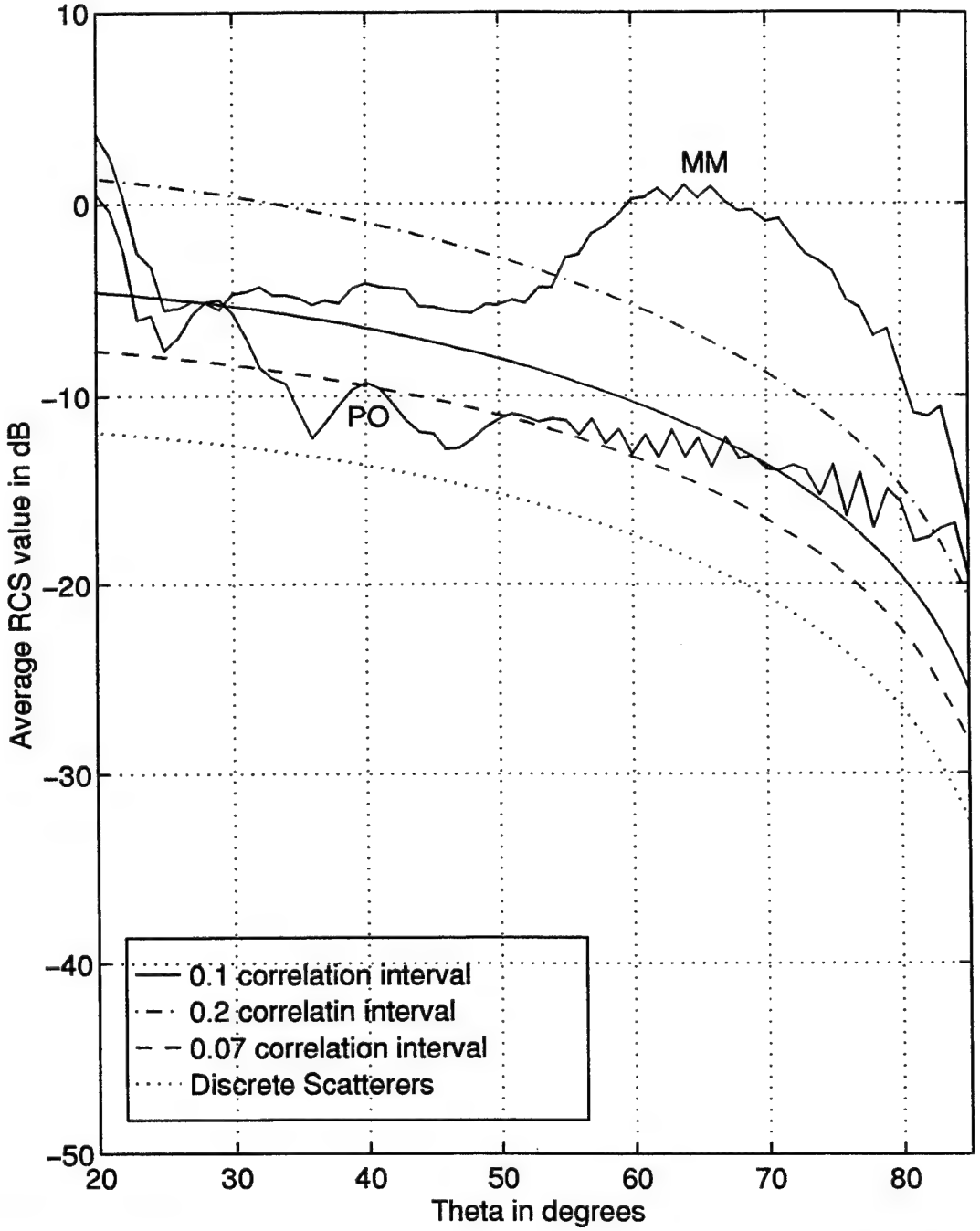

Figure 20. Comparison of the three prediction methods (MM, PO, and closed-form) for a 3λ by 3λ plate and δ_{max}= 0.1λ.

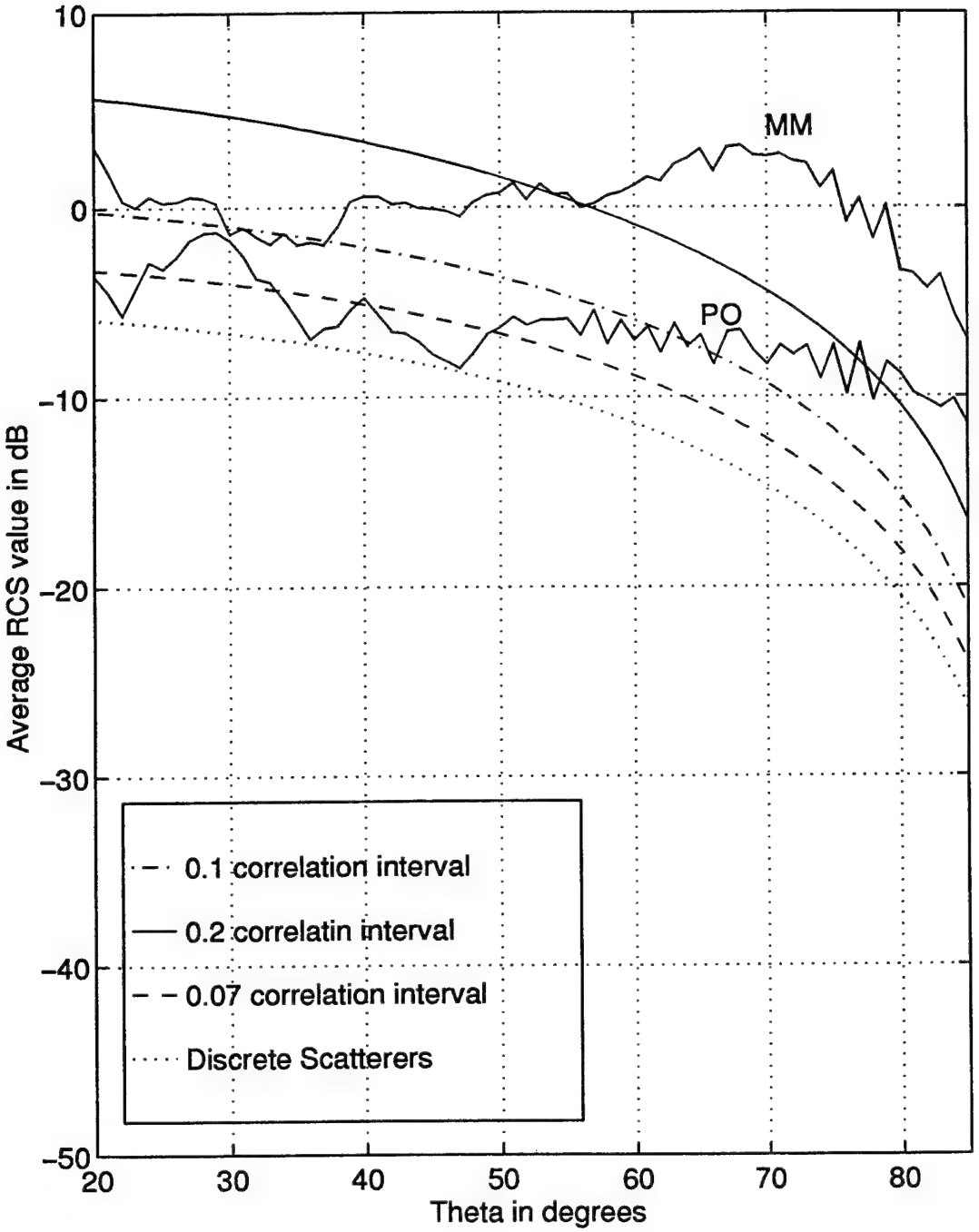

Figure 21. Comparison of the three prediction methods (MM, PO, and closed-form) for a 3λ by 3λ plate and δ_{max}= 0.2λ.

V. CONCLUSIONS AND RECOMMENDATIONS

For both MM and PO, as the surface roughness increased, so did the RCS levels in the off principal planes. Because MM is rigorous and takes into account traveling waves, it represents the most accurate modeling method. It yields higher RCS levels in the off principal plane regions than PO. However MM has several limitations that should be considered before using it. Because MM is so computationally intensive, very fast computers with large amounts of memory are required, thus limiting the size of object that can be modeled. Another factor is the amount of time one is willing to wait for results. The plates modeled in this thesis took approximately eight days of computer run time per plate on a Sparc10 with 64 Megabytes of memory. MM does provide the most accurate results but, on the other hand, the PO calculations take approximately one day. If an approximate closed-form expression could be found for the traveling wave that could be added to the PO RCS patterns, the PO approximation would be the best choice, yielding results similar to those of MM.

Ruze's closed-form expression can be used to predict the RCS in regions where diffuse scattering dominates. For the 3λ square plate there is really no angular sector where diffuse scattering dominates, and therefore the agreement with MM is not good. However, PO does not have a traveling wave lobe and therefore diffuse scattering does dominate at wide angles off the principal planes. In this case the closed-form results agree with PO if the correct correlation interval is chosen.

Future work should focus on finding an accurate closed-form expression for the traveling wave component of RCS that

can be added directly to the PO RCS. Thus the total RCS can be expressed approximately by

$$\sigma \approx \sigma_{PO} + \sigma_{DIF} + \sigma_{TW} \,. \tag{5.1}$$

That is, the total RCS is a simple summation of specular (PO), diffuse (DIF), and traveling wave (TW) terms. Equation 5.1 assumes that the sum of the fields squared is approximately the sum of the powers and this is true if only one of these terms dominates in any particular direction.

APPENDIX. COMPUTER CODE

This appendix contains the code developed to calculate RCS using the physical optics approximation. Code JPOCOS calculates the RCS pattern of a surface of random roughness. In present form, the code calculates the scattered RCS levels as a function of u and v in increments of .022 or 2/90. This creates a data string of 8281 points which can be manipulated to create a matrix of 91 by 91 data points. This data is then plotted versus u and v giving the three dimensional patterns presented in Chapter V.

```
% program POCOS.m
% latest version 7/31/95  >>> Uses geometry data from build <<<
% PO scattering from triangles
% *** has global to local coordinate transformations ***
% ****  vertices must be entered in clockwise order ****
  clear all
% Illumination flag: =0 external face only
   iflag=1;
% Geometry flag for special test cases
   Lt=.0001; % Taylor series region
   Nt=2;  % Number of terms in Taylor series
   Rs=.0;  % Surface resistivity (normalized)
   wave=1;
   bk=2*pi/wave;
   rad=pi/180;
% Incident wave polarization
   Et=1+j*0;  %TM-z
   Ep=0+j*0;  %TE-z
% Wave amplitude at all vertices
   Co=1.;
% Load data arrays generated by build
   load xpts.m
   load ypts.m
   load zpts.m
   nverts=length(xpts);
   load end1.m
   load end2.m
```

```
nedges=length(end1);
load node1.m
load node2.m
load node3.m
nfaces=length(node3);
% Load vind array which gives the three nodes for each triangle
for i=1::nfaces
   pts=[node1(i) node2(i) node3(i)];
   vind(i,:)=pts;
end
ntria=nfaces;
nvert=nverts;
x=xpts;
y=ypts;
z=zpts;
% Define position vectors to vertices
 for i=1:nvert
   r(i,:)=[x(i) y(i) z(i)];
 end
% Get edge vectors and normals from edge cross products
 for i=1:ntria
   A=r(vind(i,2),:)-r(vind(i,1),:);
   B=r(vind(i,3),:)-r(vind(i,1),:);
   C=r(vind(i,3),:)-r(vind(i,2),:);
   N(i,:)=cross(A,B);
% Edge lengths for triangle "i"
   d(i,1)=norm(A);
```

```
      d(i,2)=norm(B);
      d(i,3)=norm(C);
      ss=.5*sum(d(i,:));
      Area(i)=sqrt(ss*(ss-d(i,1))*(ss-d(i,2))*(ss-d(i,3)));
      Nn=norm(N(i,:));
      N(i,:)=N(i,:)/Nn;
      t(i,:)=cross([0 0 1],N(i,:));
      beta(i)=acos(N(i,3));
      alpha(i)=atan2(t(i,2),t(i,1)+1e-6)-pi/2;
    end
% Pattern loop
 it=0;
 for u=-1:2/90:1
    for v=-1:2/90:1
 it=it+1;
 Sth(it)=-60; Sph(it)=-60;
 if (u^2+v^2)<=1
    phi=atan2(v,u+1e-8);
    cp=cos(phi);sp=sin(phi);
    theta=asin(sqrt(u^2+v^2));
    w=cos(theta);
    st=sin(theta);ct=cos(theta);

  D0=[u v w];
       uu=ct*cp; vv=ct*sp; ww=-st;
% Spherical coordinate system radial unit vector
       R=[u v w];
```

```
% Incident field in global Cartesian coordinates
    e0(1)=uu*Et-sp*Ep;
    e0(2)=vv*Et+cp*Ep;
    e0(3)=ww*Et;
% Begin loop over triangles
    sumt=0;
    sump=0;
     for m=1:ntria
% Test to see if front face is illuminated
      ndotk=N(m,:)*R';
%    if ndotk >=0
% "local" direction cosines
   ca=cos(alpha(m)); sa=sin(alpha(m)); cb=cos(beta(m)); sb=sin(beta(m));
   T1=[ca sa 0; -sa ca 0; 0 0 1]; T2=[cb 0 -sb; 0 1 0; sb 0 cb];
   D1=T1*D0';
   D2=T2*D1;
   u2=D2(1); v2=D2(2); w2=D2(3);
% Find spherical angles in local coordinates
   st2=sqrt(u2^2+v2^2)*sign(w2);  % this makes a difference
   ct2=sqrt(1-st2^2);
   phi2=atan2(v2,u2+1e-10);
   th2=acos(ct2);
   cp2=cos(phi2); sp2=sin(phi2);
% Phase at the three vertices of triangle m; monostatic RCS needs "2"
          Dp=2*bk*((x(vind(m,1))-x(vind(m,3)))*u+...
               (y(vind(m,1))-y(vind(m,3)))*v+...
                (z(vind(m,1))-z(vind(m,3)))*w);
```

```
        Dq=2*bk*((x(vind(m,2))-x(vind(m,3)))*u+...
             (y(vind(m,2))-y(vind(m,3)))*v+...
              (z(vind(m,2))-z(vind(m,3)))*w);
        Do=2*bk*(x(vind(m,3))*u+y(vind(m,3))*v+z(vind(m,3))*w);
% Incident field in local Cartesian coordinates (stored in e2)
   e1=T1*e0';
   e2=T2*e1;
% Incident field in local spherical coordinates
   Et2=e2(1)*ct2*cp2+e2(2)*ct2*sp2-e2(3)*st2;
   Ep2=-e2(1)*sp2+e2(2)*cp2;
% Reflection coefficients (Rs is normalized to eta0)
   perp=-1/(2*Rs*ct2+1);  %local TE polarization
   para=0;                %local TM polarization
   if (2*Rs+ct2)~=0 para=-ct2/(2*Rs+ct2); end
% Surface current components in local Cartesian coordinates
  Jx2=ct2*(-Et2*cp2*para+Ep2*sp2*perp);
  Jy2=ct2*(-Et2*sp2*para-Ep2*cp2*perp);
% Area integral for general case
 DD=Dq-Dp;
 expDo=exp(j*Do);
 expDp=exp(j*Dp);
 expDq=exp(j*Dq);
 %icase(i,m)=-1;
% Special case 1
   if abs(Dp) < Lt & abs(Dq) >= Lt
    %  icase(i,m)=1;
      sic=0.;
```

```
      for n=0:Nt
       sic=sic+(j*Dp)^n/fact(n)*(-Co/(n+1)+expDq*(Co*gf(n,-Dq)));
      end
      Ic=sic*2*Area(m)*expDo/j/Dq;
% Special case 2
    elseif abs(Dp) < Lt & abs(Dq) < Lt
     %  icase(i,m)=2;
      sic=0.;
      for n=0:Nt
       for nn=0:Nt
        sic=sic+(j*Dp)^n*(j*Dq)^nn/fact(nn+n+2)*Co;
       end
      end
      Ic=sic*2*Area(m)*expDo;
% Special case 3
    elseif abs(Dp) >= Lt & abs(Dq) < Lt
     %   icase(i,m)=3;
      sic=0.;
      for n=0:Nt
       sic=sic+(j*Dq)^n/fact(n)*Co*gf(n+1,-Dp)/(n+1);
      end
      Ic=sic*2*Area(m)*expDo*expDp;
% Special case 4
    elseif abs(Dp) >= Lt & abs(Dq) >= Lt & abs(DD) < Lt
     %  icase(i,m)=4;
      sic=0.;
      for n=0:Nt
```

```
        sic=sic+(j*DD)^n/fact(n)*(-Co*gf(n,Dq)+expDq*Co/(n+1));
      end
      Ic=sic*2*Area(m)*expDo/j/Dq;
    else
      % icase(i,m)=0;
      Ic=2*Area(m)*expDo*(expDp*Co/Dp/DD-expDq*Co/Dq/DD-Co/Dp/Dq);
    end      % end of special cases test
% Scattered field components for triangle m in local coordinates
    Es2(1)=Jx2*Ic; Es2(2)=Jy2*Ic; Es2(3)=0;
% Transform back to global coordinates, then sum field
     Es1=T2'*Es2';
     Es0=T1'*Es1;
     Ets=uu*Es0(1)+vv*Es0(2)+ww*Es0(3);
     Eps=-sp*Es0(1)+cp*Es0(2);
% Sum over all triangles to get the total field
     sumt=sumt+Ets;
     sump=sump+Eps;
%    end    % end of illumination test
    end    % end of triangle loop
    Sth(it)=10*log10(4*pi*abs(sumt)^2+1.e-10);
    Sph(it)=10*log10(4*pi*abs(sump)^2+1.e-10);

   end       % end of if statement
   end       % end of pattern loop V
   end       % end of pattern loop U

   Sth(:)=max(Sth(:),-60);
```

```
Sph(:)=max(Sph(:),-60);

Sth21=Sth';
Sph21=Sph';
save Sth21.m Sth21 -ascii
save Sph21.m Sph21 -ascii
```

LIST OF REFERENCES

1. Ogilvy, J. A., *Theory of Wave Scattering from Random Rough Surfaces,* Adam Hilger, Bristol, NY, 1991.

2. Ruze, J., "Physical Limitations on Antennas," Techincal Report No. 248, MIT Research Laboratory of Electronics, October 1952.

3. Jenn, D. C., *Radar and Laser Cross Section Engineering,* American Institute of Aeronautics and Astronautics, New York, NY, 1995.

4. Moreira, F. J. and Prata, A., "A Self Checking Predictor-Corrector Algorithm for Efficient Evaluation of Reflector Antenna Radiation Integrals, " *IEEE Transactions on Antennas and Propagation,* Vol. 42, No. 2, pp. 246-253, 1994.

5. Johnson, W. A., Wilton, D. R., and Sharpe, R. M., "Patch Code Users Manual," Sandia Report No. SAND87-2991, Sandia National Laboratories, May 1988.

INITIAL DISTRIBUTION LIST

		No. Copies
1.	Defense Technical Information Center Cameron Station Alexandria, Virginia 22304-6145	2
2.	Library, Code 013 Naval Postgraduate School Monterey, California 93943-5101	2
3.	Chairman, Code EC Department of Electrical and Computer Engineering Naval Postgraduate School Monterey, California 93943-5121	1
4.	Professor David C. Jenn, Code EC/Jn Department of Electrical and Computer Engineering Naval Postgraduate School Monterey, California 93943-5121	2
5.	Professor Hung-Mou Lee, Code EC/Lh Department of Electrical and Computer Engineering Naval Postgraduate School Monterey, California 93943-5121	1
6.	John M. Waddell Route One Box 102B Westville, Florida 32464	2
7.	William Parnell 46 Test Wing/TSWM 211 West Eglin Blvd, Suite 128 Eglin AFB, FL 32542-5000	1